NASA/TM—2014-216635

Engineered Polymer Composites Through Electrospun Nanofiber Coating of Fiber Tows

Lee W. Kohlman
Glenn Research Center, Cleveland, Ohio

Charles Bakis
Pennsylvania State University, University Park, Pennsylvania

Tiffany S. Williams, James C. Johnston, Maria A. Kuczmarski, and Gary D. Roberts
Glenn Research Center, Cleveland, Ohio

February 2014

NASA STI Program . . . in Profile

Since its founding, NASA has been dedicated to the advancement of aeronautics and space science. The NASA Scientific and Technical Information (STI) program plays a key part in helping NASA maintain this important role.

The NASA STI Program operates under the auspices of the Agency Chief Information Officer. It collects, organizes, provides for archiving, and disseminates NASA's STI. The NASA STI program provides access to the NASA Aeronautics and Space Database and its public interface, the NASA Technical Reports Server, thus providing one of the largest collections of aeronautical and space science STI in the world. Results are published in both non-NASA channels and by NASA in the NASA STI Report Series, which includes the following report types:

- TECHNICAL PUBLICATION. Reports of completed research or a major significant phase of research that present the results of NASA programs and include extensive data or theoretical analysis. Includes compilations of significant scientific and technical data and information deemed to be of continuing reference value. NASA counterpart of peer-reviewed formal professional papers but has less stringent limitations on manuscript length and extent of graphic presentations.

- TECHNICAL MEMORANDUM. Scientific and technical findings that are preliminary or of specialized interest, e.g., quick release reports, working papers, and bibliographies that contain minimal annotation. Does not contain extensive analysis.

- CONTRACTOR REPORT. Scientific and technical findings by NASA-sponsored contractors and grantees.

- CONFERENCE PUBLICATION. Collected papers from scientific and technical conferences, symposia, seminars, or other meetings sponsored or cosponsored by NASA.

- SPECIAL PUBLICATION. Scientific, technical, or historical information from NASA programs, projects, and missions, often concerned with subjects having substantial public interest.

- TECHNICAL TRANSLATION. English-language translations of foreign scientific and technical material pertinent to NASA's mission.

Specialized services also include creating custom thesauri, building customized databases, organizing and publishing research results.

For more information about the NASA STI program, see the following:

- Access the NASA STI program home page at *http://www.sti.nasa.gov*

- E-mail your question to *help@sti.nasa.gov*

- Fax your question to the NASA STI Information Desk at 443–757–5803

- Phone the NASA STI Information Desk at 443–757–5802

- Write to:
  STI Information Desk
  NASA Center for AeroSpace Information
  7115 Standard Drive
  Hanover, MD 21076–1320

NASA/TM—2014-216635

Engineered Polymer Composites Through Electrospun Nanofiber Coating of Fiber Tows

Lee W. Kohlman
Glenn Research Center, Cleveland, Ohio

Charles Bakis
Pennsylvania State University, University Park, Pennsylvania

Tiffany S. Williams, James C. Johnston, Maria A. Kuczmarski, and Gary D. Roberts
Glenn Research Center, Cleveland, Ohio

National Aeronautics and
Space Administration

Glenn Research Center
Cleveland, Ohio 44135

February 2014

Level of Review: This material has been technically reviewed by technical management.

Available from

NASA Center for Aerospace Information
7115 Standard Drive
Hanover, MD 21076–1320

National Technical Information Service
5301 Shawnee Road
Alexandria, VA 22312

Available electronically at http://www.sti.nasa.gov

Engineered Polymer Composites Through Electrospun Nanofiber Coating of Fiber Tows

Lee W. Kohlman
National Aeronautics and Space Administration
Glenn Research Center
Cleveland, Ohio 44135

Charles Bakis
Pennsylvania State University
University Park, Pennsylvania 16802

Tiffany S. Williams, James C. Johnston, Maria A. Kuczmarski, and Gary D. Roberts
National Aeronautics and Space Administration
Glenn Research Center
Cleveland, Ohio 44135

Abstract

Composite materials offer significant weight savings in many aerospace applications. The toughness of the interface of fibers crossing at different angles often determines failure of composite components. A method for toughening the interface in fabric and filament wound components using directly electrospun thermoplastic nanofiber on carbon fiber tow is presented. The method was first demonstrated with limited trials, and then was scaled up to a continuous lab scale process. Filament wound tubes were fabricated and tested using unmodified baseline towpreg material and nanofiber coated towpreg.

Introduction

Composite materials are typically constructed of a fiber and matrix, with the fiber placed at various angles and positions within the matrix. In a unidirectional laminate, the strength of the material is primarily determined by the strength of the fiber, strength of the matrix, adhesion of the fiber to the matrix, fiber volume fraction, and the presence of defects. Since the fiber direction strength relies on load carried by the fiber, the lamina is much stronger in the fiber direction than in any direction orthogonal to the fibers. Multi-directional laminates use many unidirectional lamina layers at different orientations to combine the high fiber direction strength with the low transverse strength to achieve suitable bulk properties. These materials rely on the transfer of shear loads across an interface between the lamina. Ultimately, when this interface fails, the composite will likely fail. Features such as edges, holes, or delamination due to damage often serve as the initiation point for the failure of the interface. Components with more complex architectures such as those produced with fabrics including weaves or braids, or by filament winding limit the propagation of catastrophic delamination by limiting the continuity of the interface planes. However, failure often still results from interface failure. Toughening of the interface can be used to increase the durability and strength of composite structures by suppressing the delamination of the interface. Andersons (2004) discusses the role of interface damage propagation and toughness in overall composite failure and frames well the motivation for the approach that has been taken in this work.

Toughening and other property enhancements of composite materials are typically implemented by modifying the bulk properties of the constituents, either the fiber or matrix materials. This often leads to difficulties in processing and higher material costs. Many composites consist of tows or yarns (thousands of individual fibers) that are either filament wound or processed into a fabric by weaving or braiding. The matrix material can be added to the tow or fabric before final processing, resulting in a prepreg material,

or infused into the fiber material during final processing by a variety of methods. By using a direct electrospun deposition method to apply thermoplastic nanofiber to the surface of the tows, the tow-tow interface in the resulting composite can be modified while using otherwise conventional materials and handling processes. Other materials of interest could also be incorporated into the electrospun precursor.

Approach

Early work demonstrated the feasibility of directly depositing electrospun nanofibers onto continuous carbon fiber materials. Additional work consisted of three parts. The first was design and construction of a device for continuously depositing electrospun thermoplastic nanofiber onto larger quantities of carbon fiber prepreg tow. The second part involved the production of the modified tow material and fabrication of filament wound composite tubes. Tubes were fabricated at Pennsylvania State University with two fiber orientations using both the original tow and the modified material. The third part of the work involved characterization and testing of the fabricated tubes to evaluate the effects of the nanofiber toughening on mechanical properties.

Electrospinning Method

The electrospinning method is a process in which a precursor material is formed into a thin filament by electrostatic forces. The fibers produced can be on the nanometer scale. First, the fiber material is chosen and dissolved in a solvent. Typically, thermoplastic polymers are used. A high electric potential is then applied to the solution. The electrostatic forces stretch the solution into a Taylor cone which then forms a jet that elongates and solidifies as the solvent evaporates. The charged fibers are then collected on a grounded or oppositely charged target. As the fiber stretches it becomes unstable. This results in a random fiber placement. The solution can be handled in several different ways including passing the solution through a needle or porous foam, or by rotating a partially submerged roller in a bath of precursor solution. Figure 1 is a simple sketch of the electrospinning process using a needle.

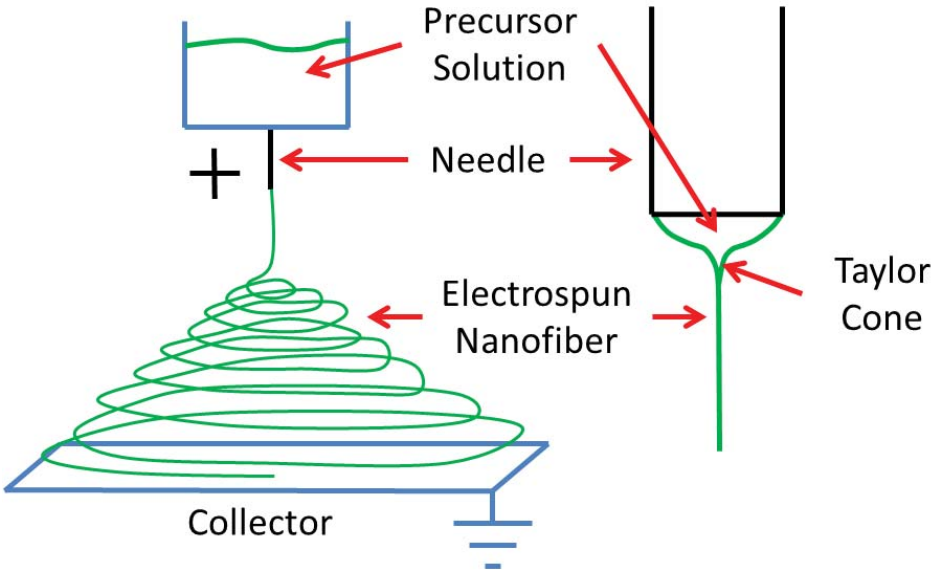

Figure 1.—Basic sketch of electrospinning process.

Many different variables can affect the electrospun fiber. Some of these include solution viscosity, surface tension, solvent vapor pressure, ambient solvent vapor pressure, humidity, electric potential, polymer mechanical properties, solution conductivity, target and solution delivery geometry, temperature, and ambient gas flow conditions such as cross flow or turbulence. Bhattacharjee (2011) provides a comprehensive overview of the electrospinning process and the many variables involved.

Early Work

Early work performed during a Glenn Research Center Innovation Fund Fast Track project in 2011 demonstrated the feasibility of directly electrospinning fiber onto a carbon fiber tow. A solution of 15 percent by weight polyethersulfone (PES) dissolved in dimethylformamide (DMF) was selected as the nanofiber precursor. PES was selected for this early work for its mechanical properties and availability. The solution was supplied to a circular array of eight stainless steel 16 gauge flat tip needles. Flow to the needles was controlled by manifold with a series of needle valves. A peristaltic pump was used to supply solution to the manifold. Polypropylene and silicone tubing were used for transport of the electrospinning precursor solution. Homaeigohar (2010) and Tang (2009) provide more information on electrospinning of PES.

A potential of 20 kV was applied to the needles by charging the needle support ring. This ring was electrically isolated by suspending it from silicone tubing within a large fume hood. To create the coating on the carbon fiber tow, the electrospun nanofibers (still positively charged) were collected electrostatically on a grounded carbon fiber tow passing through the center of the needle array. The carbon tow was diverted through the needle array from the original path through a tow coating and winding machine (existing equipment that was borrowed for this test) using pulleys attached to the ventilation hood by magnets. The coated carbon fiber tow was slowly pulled through the electrospinning needle array and collected continuously on the winding machine's rotating drum.

Figure 2 (left) shows large clumps of nanofiber forming and depositing on the surface of the grounded carbon fiber tow running vertically through the center of the needle ring (indicated by red oval). The image on the right is the solution supply pump and manifold.

Scanning electron microscopy (SEM) images of the resulting fibers on the surface of a carbon fiber tow at 500x (left) and 2000x (right) are shown in Figure 3. Typical diameters are in the 50 to 250 nm range. The beads observed in the SEM images are likely the result of either incomplete dissolution of the PES powder, too low of a dissolved polymer fraction in the solution, or both. Electrospinning with a solution having too low of a viscosity often results in electrospraying rather electrospinning which produces very small droplets. Initial attempts at obtaining the target 20 percent solution were unsuccessful due to solvent saturation and subsequent PES precipitation. Typically, PES would be very soluble in DMF, however the PES used in this project was obtained from a readily available sample batch that was chemically functionalized.

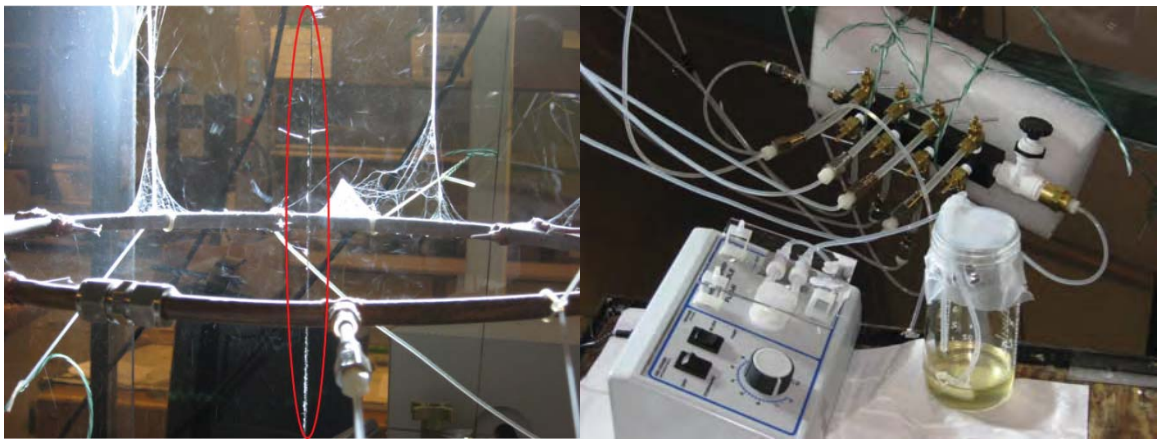

Figure 2.—Nanofibers accumulating on the carbon fiber tow (left), polymer solution supply (right).

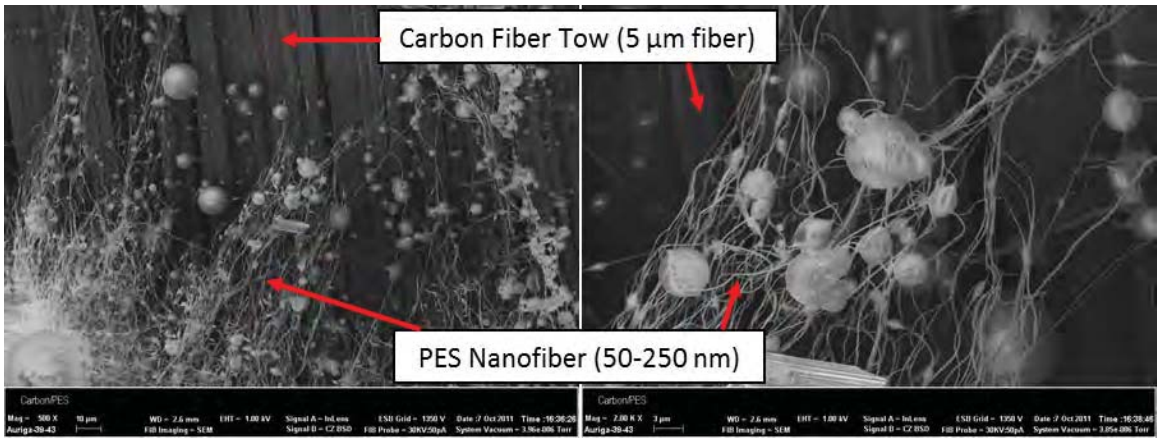

Figure 3.—PES nanofiber on the surface of a carbon fiber tow at 500x (left) and 2000x (right).

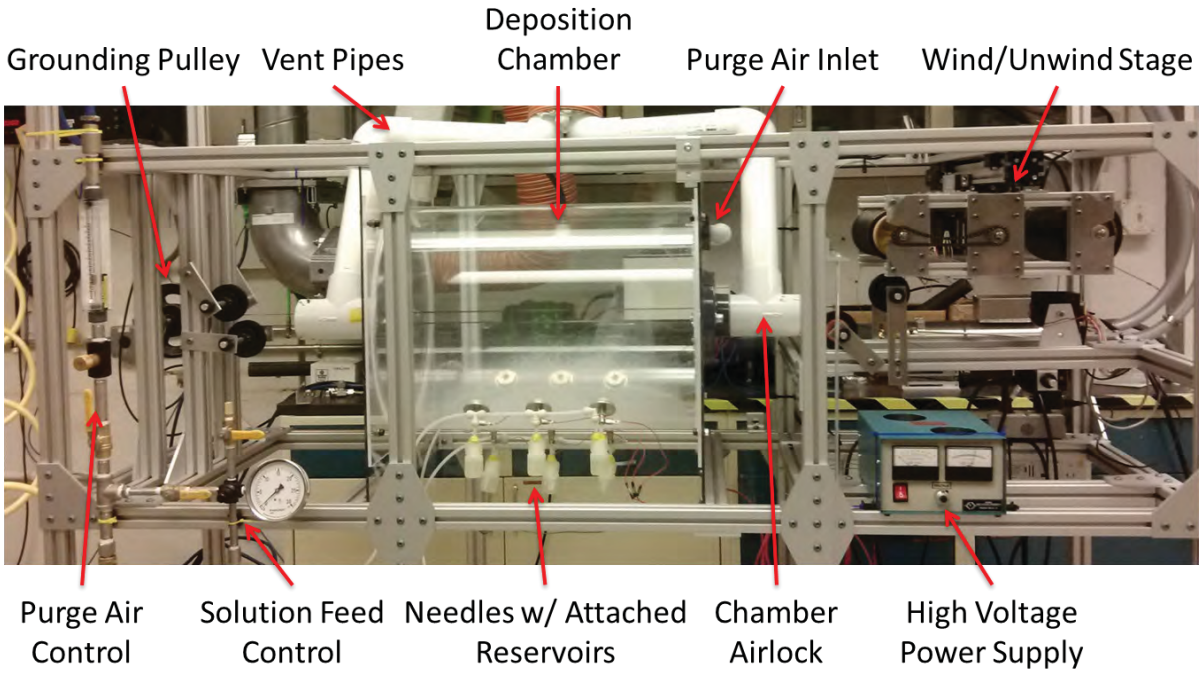

Figure 4.—Electrospun nanofiber deposition machine.

The results of this early work were used in a proposal for additional funding under the ARMD Seedling Fund in 2012. The results of which will be discussed in the following sections.

Electrospun Deposition Machine

Following the successful demonstration of the deposition method, additional work was proposed and funded by NASA's ARMD Seedling Fund. The first portion of this new work focused on the development of a machine to produce several thousand meters of nanofiber coated tow prepreg. The machine that was built consists of two main sections, the winding stage and the deposition chamber. Figure 4 shows an overview of the machine.

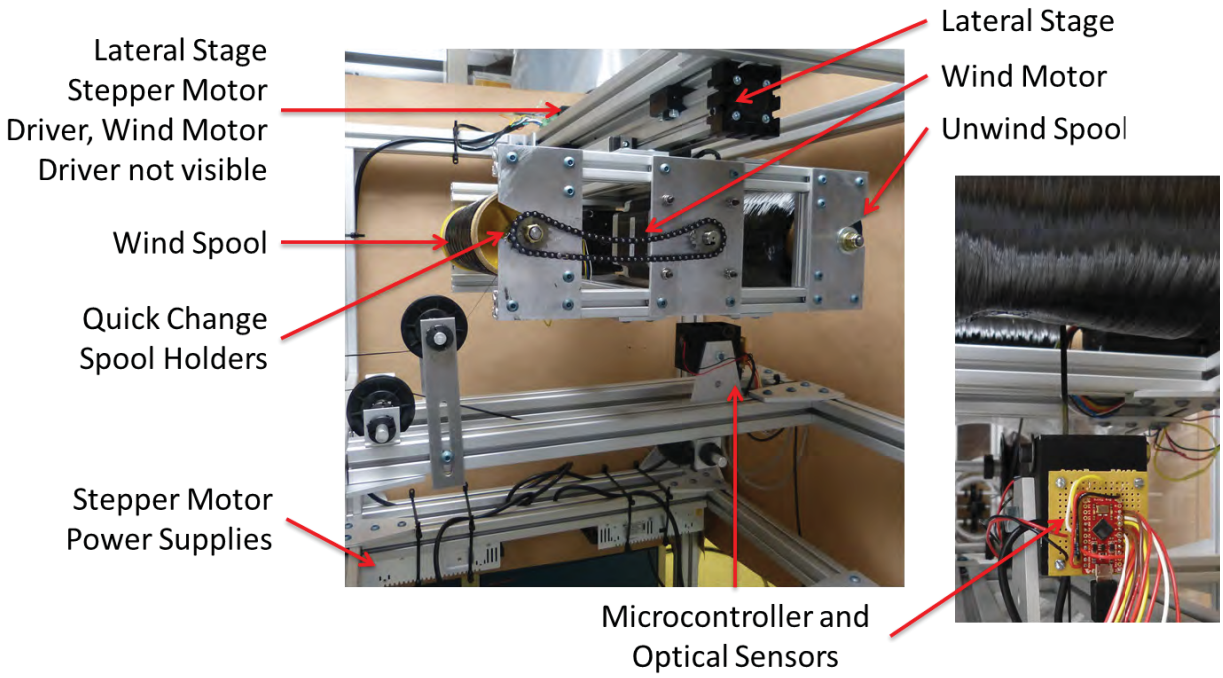

Figure 5.—Carbon fiber wind/unwind stage.

The wind/unwind stage holds two cardboard carrier spools. The uncoated spool is located on the right in Figure 5. A motor with shorted windings applies drag to the spool through a chain and sprocket (rear, not visible). The carbon tow passes between a pair of LED's and a pair of photoresistors as it comes off the spool. A microcontroller monitors the voltage ratio on the photoresistors and provides control signals to the wind motor and the lateral stage motor. In this way, the entire stage is controlled to ensure the carbon tow is fed straight onto the pulleys, through the machine, and onto the wind spool with the same wind angle as the original spool. The cardboard carrier tubes are held in place using a pair of pipe test plugs on a length of all-thread; a pipe test plug consists of two opposed conical disks that when compressed expand a rubber ring into contact with the inner diameter of the tube. Flanged bearings hold the all-thread and tube assembly in place in slanted notches to allow the assembly to be easily removed and the spool quickly changed.

The unwound tow then passes through the deposition chamber shown in Figure 6. The deposition chamber is a transparent plastic tube with plates on each end. Two fittings on each end plate provide purge air and allow the tow to pass into the chamber. An airlock is formed by using a "T" fitting with the intersecting side connected to the ventilation system. This way, the fiber can pass into the chamber and the chamber atmosphere can be controlled. The purge air forces the solvent vapors out of the chamber and into the ventilation system through the airlocks. Also, since the ventilation system operates at a higher flow rate than the purge air, solvent vapors do not enter the room and the room air does not enter the chamber.

The polymer precursor solution is held in nine small bottles located at the bottom of the chamber. Each bottle was slightly pressurized (around 1 psi or 7 kPa) to force the solution up a dip tube and through a 22 gauge, 2 in. (50.8 mm) long stainless steel needle. A high strength rare earth magnet inside the chamber and a large fender washer located at the base of the needle was used to hold the needle with attached reservoir, tubing, and wiring in place. A high voltage power supply was used to apply an electric potential of between 20 and 25 kV to the needles.

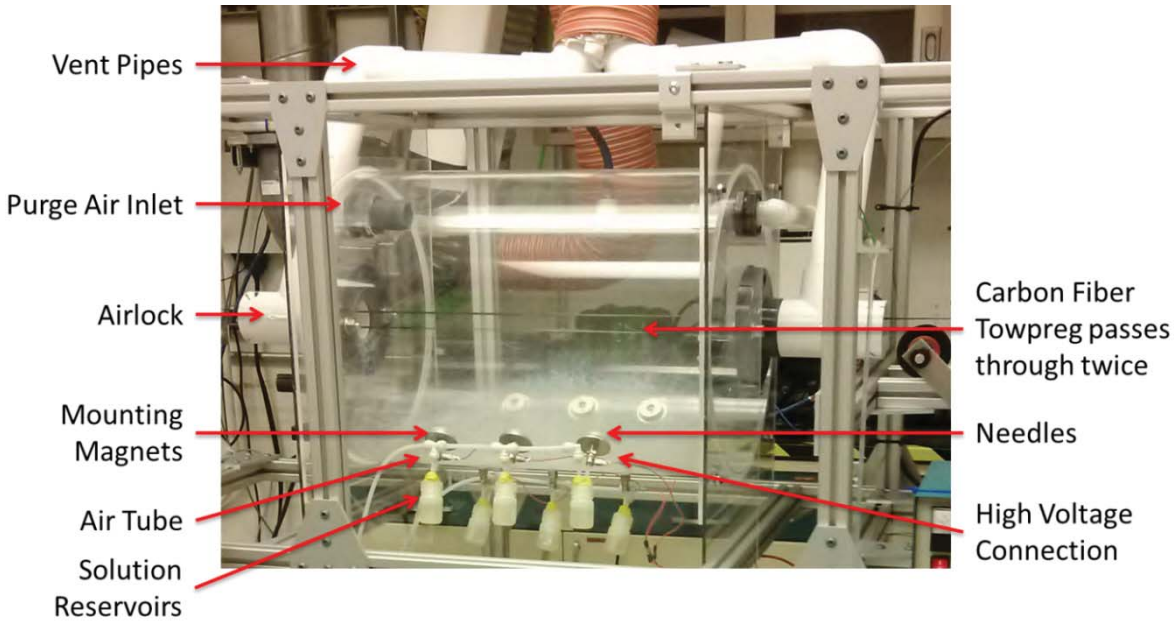

Figure 6.—Electrospun deposition chamber.

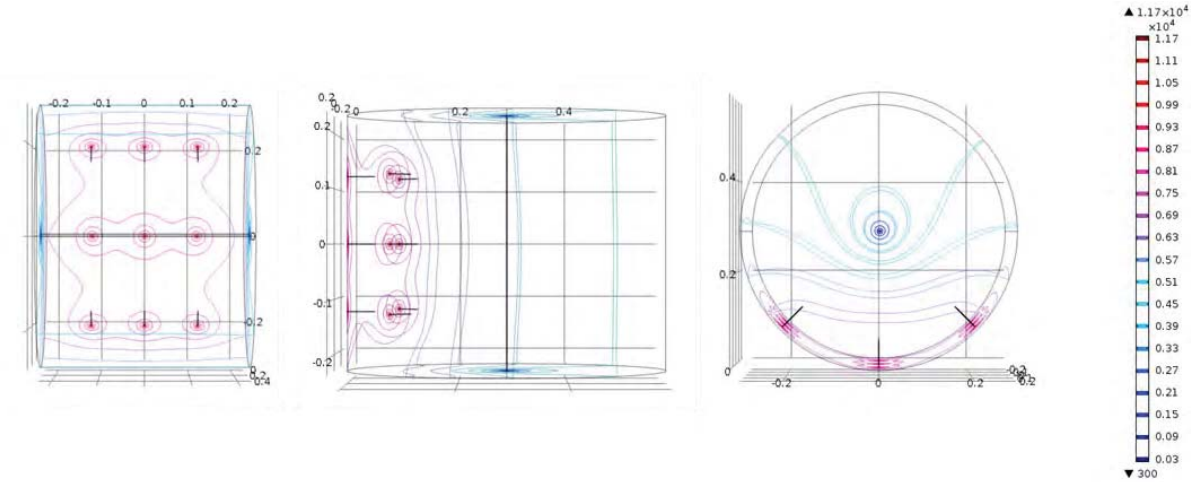

Figure 7.—Contour plots of electric potential for the selected needle array on the inner chamber surface, scale bar shows voltage, 20 kV applied to the needles.

The array of electrospinning needles was chosen to be located on the bottom of the chamber to minimize the possibility of droplets reaching the carbon tow. In earlier work in which the fiber was positioned vertically, large droplets of solution would deposit on the tow when the droplet at the opening of the needle would occasionally detach. An array consisting of nine needles provided a balance of electric field overlap and electrospun nanofiber production rate. COMSOL software was used to investigate a range of needle placements and needle numbers within the constraints of the chamber volume. Figure 7 shows the electric potential resulting from the selected array.

The deposition chamber is an 18 in. (457 mm) OD acrylic tube with a 1/4 in. (6.35 mm) wall, 24 in. (609 mm) long. Polycarbonate end plates cover the ends and hold the ports for the purge air and airlock assemblies. Three rows of three needles each are supported by rare earth magnets and are positioned along the bottom, and 45° up the circumference of the tube. The needles are spaced 12 cm apart along the axis of the tube and the middle needle is centered. The rare earth magnets are held in place with silicone adhesive.

Nanofiber Precursor Material Preparation

Nylon 11 was selected for electrospinning due to its toughness and chemical resistance to most solvents. Nylon particles have also been considered as a matrix toughener for epoxies, and the use of electrospun nylon nanofiber mats as an interleaving material is believed to have the potential to improve the in-plane properties by bonding with the resin and reinforcement. Results from electrospinning nylon 11 and nylon 6 nanofibers have been reported, but attempts to dissolve nylon in low toxicity solvents with low boiling points have not been successful due to polyamide being amphiphilic, which often makes this material difficult to use during large batch processing.

Initial experimental efforts included dissolving nylon 11 pellets in a variety of solvents, with a heated solution of benzyl alcohol being the only solvent where nylon 11 was completely soluble. Unfortunately, when the solution cooled to room temperature the nylon recrystallized and the mixture turned into a waxy-like consistency. Salts and other additives were incorporated into the solution during the mixing process as an attempt to reduce the hydrogen bonding and allow nylon 11 to remain suspended in solution at room temperature, but none of those methods worked. Eventually, a procedure was adopted from Behler et al., and a 2.5 wt% nylon 11 electrospinning solution was successfully prepared from a mixture of three parts dichloromethane and one part formic acid (Behler, 2007).

Nanofiber Deposition Machine Operation

Carbon fiber towpreg was purchased from TCR Composites (Ogden, UT). The towpreg is made with T700SC-12K carbon fiber tow and B-staged UF3325 epoxy. The full spool was mounted on the unwind stage using the removable holder and expansion pipe test fittings. The end of the towpreg was pulled slowly from the spool by hand and fed through the optical position sensor/controller and around the first two guide pulleys. The wind controller was then powered on to maintain the spool position while the tow was pulled through the deposition chamber, around the grounding side pulleys, through the chamber, around the exit pulleys and onto the winding spool. The free end was wrapped around the winding spool and under the next wind to hold it in place.

The tubing connecting the dip tube and air supply were sealed to the caps of the solution reservoirs using tacky tape, typically used in vacuum bagging operations. The reservoirs were then filled and the needles, with attached fender washers, and air lines connected. The mounting magnets supported the reservoirs and tubing while positioning the spinning needle. The high voltage connection was attached using a wiring harness with nine electrical clips and the safety shield panels were put into place.

The ventilation was continuously operating, however operation was checked before start up. Once the needles, reservoirs, and tow were in place, the purge air was adjusted to 6 CFM (170 l/min) and inward flow at the airlock opening was verified. Then the winding controller was started and the high voltage supply turned on and set to 22.5 kV. The winder was set to run at 10 rpm. The resulting material throughput was roughly 8.5 ft/min (2.59 m/min); the linear speed increases as the material on the wind spool gets thicker and the radius increases. The final step was to start the solution flow. The air pressure supply valve was opened with the regulator turned to zero and the vent valve open. The vent valve was slowly closed, ensuring that the regulator maintained zero pressure, then the pressure was slowly increased until solution was seen at the tips of the needles. The pressure required for sufficient flow was typically around 1 psi (7 kPa), and always less than 2 psi (14 kPa). The pressure was adjusted to maintain droplets at the tips of several needles while avoiding splattering or running of the solution down the needle. The voltage also needed to be adjusted slightly (always between 20 and 25 kV) to maintain at least three needles operating correctly.

Due to slight variations in each needle and reservoir, stable and sufficient flow to all nine needles was not possible. During the first few minutes of operation, most needles would electrospin, producing large amounts of nanofiber that would clump before depositing on the carbon tow. This was followed shortly by plugging of several needles from insufficient solution supply. Increasing the supply pressure would result in splattering and solution streaming down some of the needles. Steady state operation of the

machine would result soon after and the three electrospinning needles continued to function until reservoirs emptied, typically after 1 to 1.5 hours of operation. Each reservoir had a capacity of 30 mL.

When the reservoir needed to be refilled, the solution air supply valve was first turned off, then the supply vent valve opened. The high voltage supply was then turned off and the winding controller turned off. The bottles were then unthreaded from the caps, filled, and replaced. The winding controller was then turned on, the high voltage supply turned on to the previous setting, the solution air supply turned on, and the vent valve slowly closed. Any adjustments would then be made to the voltage and solution air supply pressure to maintain stable operation of three needles.

Further work is needed to improve the current system. One possible solution is to use one pressure regulator for each needle instead of the common supply so that each needle could be adjusted individually. Individual needle control was attempted by regulation the solution flow of each needle in the earlier work, but the conductivity of the solution made adjustment during operation impossible because the valves were all charged to high potential. The use of the air pressure flow control system allowed the flow to be safely adjusted during operation. Figure 8 is a video of nanofiber deposition during operation. The carbon fiber towpreg is visible in the center of the chamber and the electrospinning needles are at the bottom. Small clumps of nanofiber can be seen depositing on the carbon towpreg as it passes twice through the chamber. After several hours of operation, a cobweb like structure is visible at the top of the chamber. This was formed by nanofiber that drifted upward into the purge air streams entering from the sides at the top of the chamber.

Four batches of nanofiber coated material were produced. The first trial batch was used to adjust operation of the machine. The following three batches, consisting of roughly 12,000 ft (3658 m) of coated material produced during over 20 hours of total operation, were used to fabricate the coupons for comparison with the uncoated material.

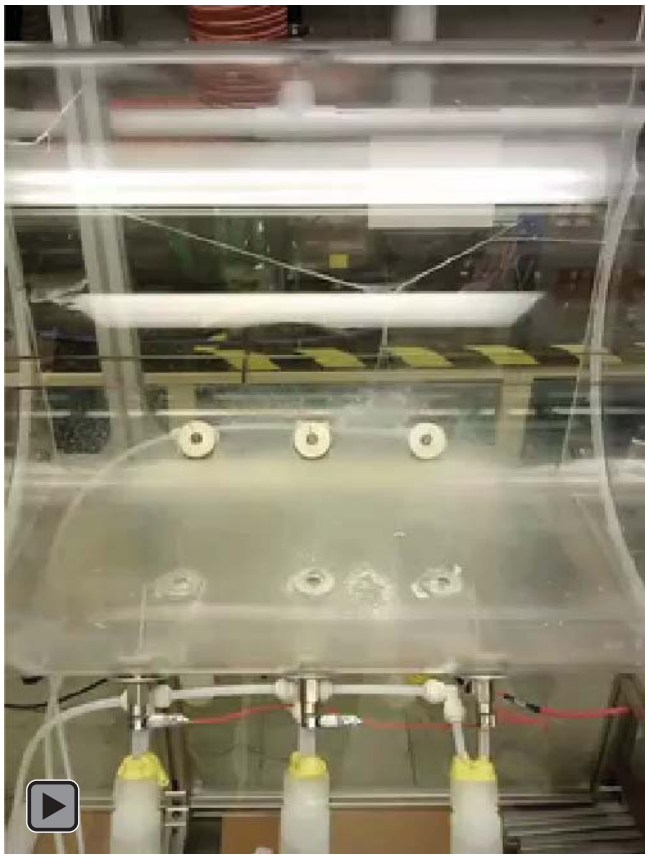

Figure 8.—Video of nanofiber deposition during operation.

Coupon Fabrication

Coupons were fabricated by Pennsylvania State University (PSU) under the direction of Dr. Charles Bakis, Grant Number NNX12AR01A. This section discusses the tubes produced at PSU, manufacturing method, some information on quality and prediction of mechanical properties of the specimens using ply-level stress analysis.

Baseline Tubes

This section describes 90° and ±45° baseline (unmodified) carbon/epoxy tubes made at Penn State for NASA's testing program.

Aluminum mandrels with hemispherical end domes were used for making the tubes. The mandrels having 48.26-mm (1.9 in.) outer diameter were coated with two coats of Monocoat E340 release agent. Each coat of release agent was baked at 121 °C (250 °F) for 1 hr.

All the tubes were wound using a single pre-impregnated tow (towpreg). During the entire winding process, tow tension was kept at 22.2 N (5 lb) and temperature of the part was kept at 66 °C (150 °F) using a radiant heater coupled with an infrared thermometer and digital temperature controller. Photographs of the winding process are shown in Figure 9.

In order to achieve a wall thickness near 2.5 mm (0.1 in.), hoop-wound tubes were made with nine coverages with a circumferential pattern (each stroke is a coverage with a circumferential pattern). Likewise, the ±45° tubes were made with four helical pattern coverages (each coverage is a ±θ layer in a helical pattern). A helical pattern of five was used in ±45° tubes—meaning there are five rhombic patterns around the circumference of the tube. After the layers were wound, Dunstone 220R brand shrink-tape (Charlotte, NC) was circumferentially wound onto the parts with a 50 percent overlap. Following the application of shrink-tape, the parts were placed stationary in an oven and cured at 143 °C (290 °F) for 2 hr. A photograph of a cured part, prior to removing the shrink tape, is shown in Figure 10.

After cure, the shrink tape was peeled off and the tubes were cut into specimens having 20.3 cm (8 in.) and 7.6 cm (3 in.) lengths for tension and compression testing, respectively. Photographs of compression specimens are shown in Figure 11. The shallow spiral imprint seen on the surface of both tubes is caused by the shrink tape.

Longitudinal cross sections of the tubes were cut, lightly polished, and inspected in an optical microscope to check the quality of the specimens. Typical photomicrographs are shown in Figure 12. Nothing out of the ordinary was observed in these inspections.

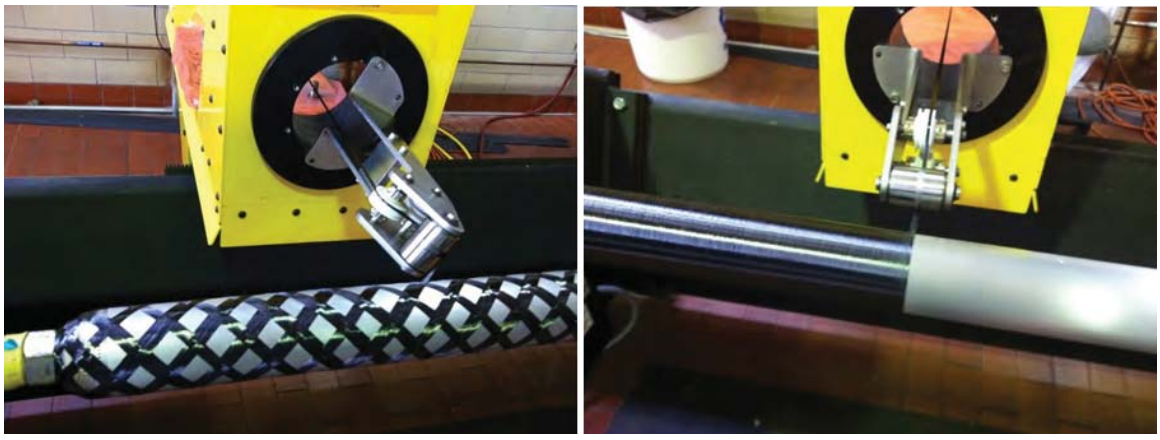

Figure 9.—Photographs of filament winding process, ±45 (left) and 90 (right).

Figure 10.—Photograph of cured hoop-wound tube wrapped in shrink tape.

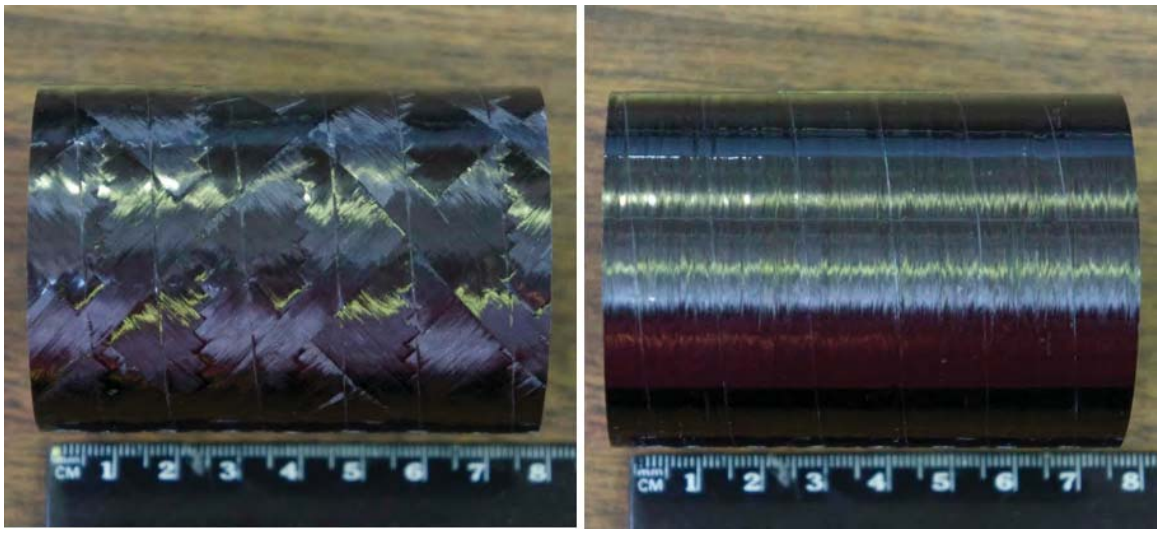

Figure 11.—Photographs of finished specimens, ±45 (left) and 90 (right).

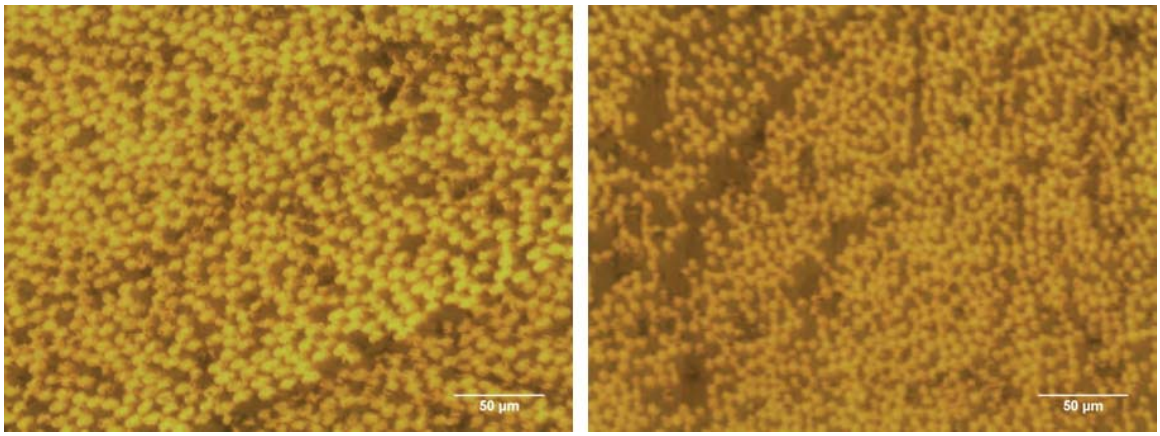

Figure 12.—Photomicrographs of longitudinal cross-sections of specimens, ±45 (left) and 90 (right).

Significant variation in the wall thickness was observed in the ±45° specimens (Figure 13). No correlation was observed between the thickness variation and the location of the specimen on the mandrel, the position of the measurement on the helical winding pattern, or even the method of winding the shrink tape (i.e., by hand or using an apparatus that precisely controlled pitch and tension). Further investigation would therefore be required to determine the cause of the variation. It was decided to use these tubes for testing in spite of the thickness variation. The average difference between the thickest part of the wall and the thinnest part of wall was 0.25 mm in the ±45° specimens and 0.09 mm in the hoop-wound specimens. Appendix A summarizes wall thickness measurements made at the top and bottom ends of each specimen. Classical laminated plate theory (CLPT) was used to predict the mechanical properties of the tubes under the thin-wall assumption (i.e., the wall's properties are calculated as if the material was a flat plate). This approximation is considered appropriate since the wall thickness is roughly a tenth of the tube radius. Since a full set of elastic and strength properties for the TCR towpreg could not be found, best-guess estimates for a T700/epoxy composite were employed for the calculations. The estimated ply properties are listed in Table 1 and the estimated properties for the $[\pm 45]_4$ and $[90]_9$ tubes are listed in Table 2 and Table 3, respectively.

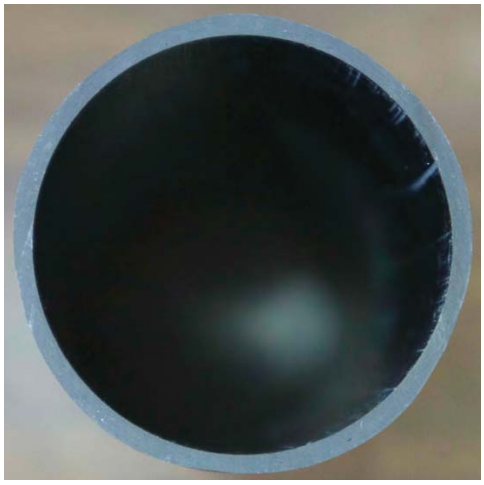

Figure 13.—End-view of a ±45 specimen showing wall thickness variation.

TABLE 1.—ESTIMATED PLY PROPERTIES FOR UNIDIRECTIONAL T700/EPOXY, USED FOR CLPT PREDICTIONS OF TUBE PROPERTIES

Longitudinal modulus	E_1 (GPa)	153
Transverse modulus	E_2 (GPa)	10.5
Longitudinal poisson's ratio	ν_{12}	0.3
Shear modulus	G_{12} (GPa)	8.27
Longitudinal tensile strength	F_{1t} (MPa)	2760
Longitudinal compressive strength	F_{1c} (MPa)	781
Transverse tensile strength	F_{2t} (MPa)	76.5
Transverse compressive strength	F_{2c} (MPa)	233
Shear strength	F_6 (MPa)	89.6

TABLE 2.—ESTIMATED PROPERTIES OF [±45]4 T700/EPOXY TUBES

Nominal OD (mm)	52.95
Nominal ID (mm)	48.26
Area (mm^2)	373.1
Mom. inert (mm^4)	239400
Tensile strength (MPa) (kN)	179 66.9
Compressive strength (MPa) (kN)	176 65.6
Torsional strength (MPa) (N-m)	290 2620
Axial modulus (GPa)	27.7
Shear modulus (GPa)	39.6
Axial poisson's ratio	0.68

TABLE 3.—ESTIMATED PROPERTIES OF $[90]_9$ T700/EPOXY TUBES

Nominal OD (mm)	52.77
Nominal ID (mm)	48.26
Area (mm^2)	358.1
Mom. inert (mm^4)	228900
Tensile strength (MPa) (kN)	76.5 27.4
Compressive strength (MPa) (kN)	233 83.5
Torsional strength (MPa) (N-m)	89.6 778
Axial modulus (GPa)	10.5
Shear modulus (GPa)	8.27
Axial poisson's ratio	0.021

Modified Tubes With Preliminary Modified Tow

This section summarizes the winding characteristics of a preliminary batch of coated carbon/epoxy towpreg received on June 13, 2013. The outermost tow was marked clearly and seemed to unspool without any problem at the beginning of the winding process. But after a few passes, it was realized that the tow was not unspooling freely. When the process was stopped and the spool was taken out of the winder, it was seen that the outermost fiber could not unspool freely due to the restriction of the fibers that are crossing over it, as shown in Figure 14. As the outermost tow was pulled during winding, it cut the fibers that are crossing over it causing the occurrence of open-ended fibers as seen in Figure 15. This problem became more severe as the tow was allowed to cut more fibers and the number of the open-ended fibers accumulated. The problem was solved by manually cutting all the fibers that were crossing over the outermost tow, and by removing all of the open-ended fibers. This same behavior was also observed during unwinding of the spool during deposition of the nanofiber and was likely more severe in the modified tow due to rewinding. Performing the nanofiber deposition in line with the resin impregnation process would reduce or eliminate this problem.

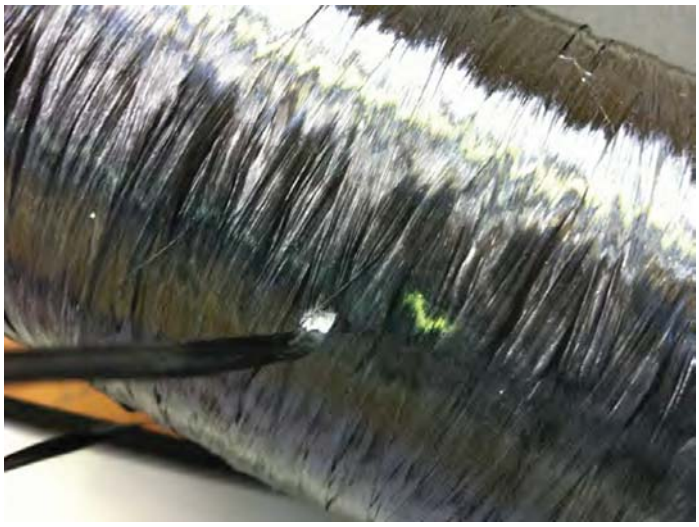

Figure 14.—Fibers crossing over the outermost tow.

Figure 15.—Open ended fibers.

Another behavior that was observed was the presence of small-diameter white colored fibers that did not stick well to the tow. This was observed right after the tow came out of the spool. These fibers are clumps of nanofiber that were deposited on the tow. The rollers of the filament winder did not seem to aggravate this "shedding" behavior, so we do not believe that it is a major problem. The cutting of tow required by the splitting behavior shown in Figure 15 is likely to be problematic for winding full mandrels in the future. This is likely due to handling of the tow either in the initial tow impregnation, shipping, or unwinding for nanofiber deposition as this was observed to a lesser extent during deposition unwinding.

Some parts of the coated carbon/epoxy towpreg contained dark yellow colored regions, as seen in Figure 16. This is due to clumping of the nanofibers during the deposition process. The first few meters of the unspooled towpreg seemed to have a smaller and more variable tow width compared to the rest of the spool and the previously sent non-coated carbon/epoxy towpreg. After the first few meters, the tow width was consistent. It would be best if the cause of the tow width variation were eliminated so that the quality of the manufactured parts can be maximized. Filament winding relies on a consistent tow width for an optimal, homogeneous microstructure inside the composite.

A 90° compression specimen was wound with the limited amount of coated towpreg provided by NASA in this batch. Figure 17 shows optical microscope pictures of a polished cross-section, with the plane of the cut perpendicular to the fibers. At these magnifications, it is not possible to see the electrospun fibers in the matrix.

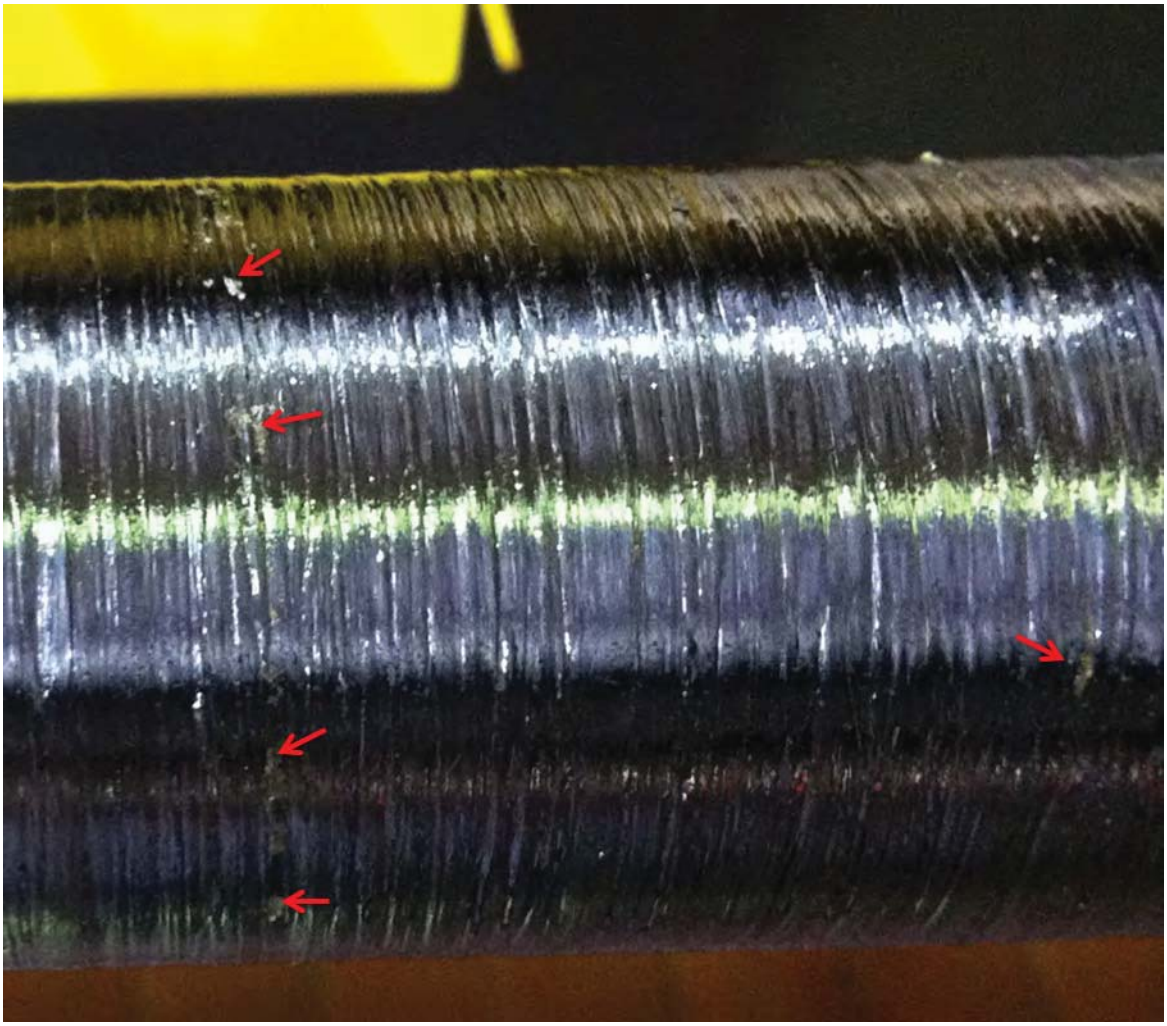

Figure 16.—Yellow colored regions on the towpreg, highlighted with arrows.

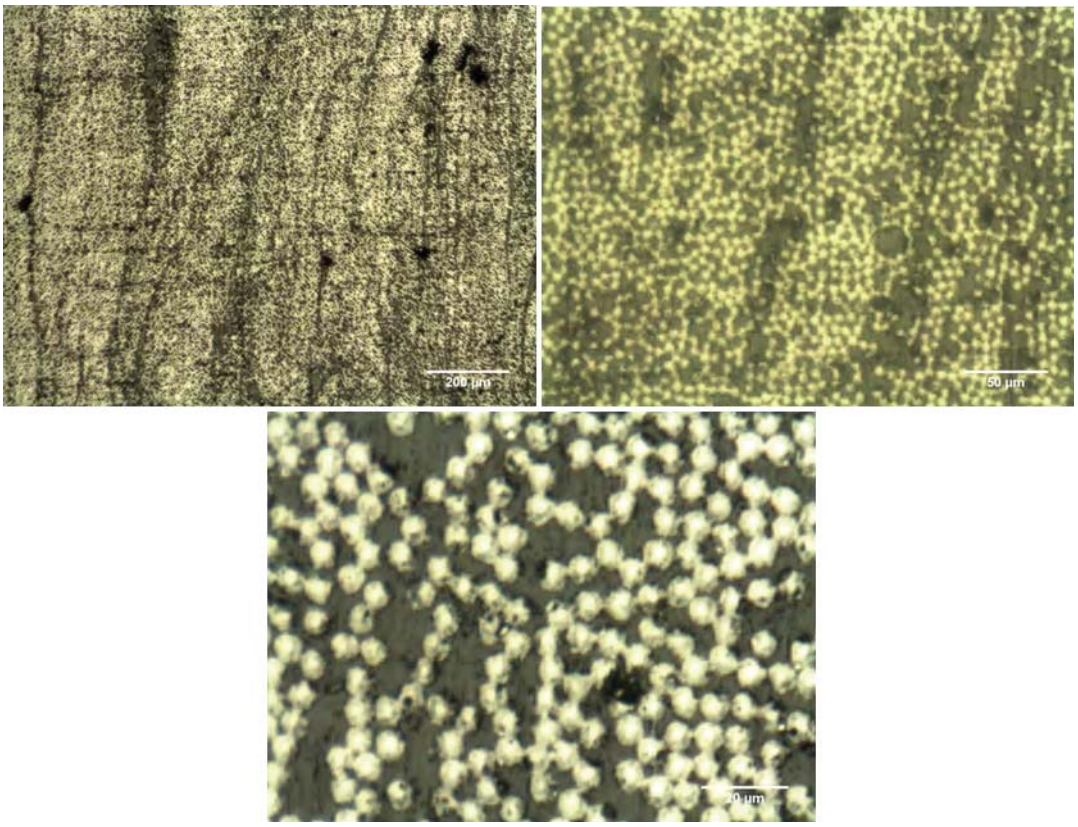

Figure 17.—Optical microscope images of polished cross-section from 90° specimen, sectioned perpendicular to fibers, higher magnification from top left, to top right, to bottom.

TABLE 4.—SUMMARY OF BATCHES OF TOWPREG

Batch no.	Date received at PSU
2	June 26, 2013
3	June 27, 2013
4	July 11, 2013

Modified Tubes With Production Modified Tow

This section summarizes the 90° and ±45° modified (nanofiber-coated) carbon/epoxy tubes made at Penn State for NASA's testing program. The coated tow was received in three batches (Table 4).

Batch 1, received on June 13, 2013 was used to do a 90° trial wind, as reported in the previous section. It was mentioned that loose (broken) fibers caused unspooling problems, which necessitated occasionally cutting off layers of fiber from the spool while winding. Batches 2, 3, and 4—the subject of the present section—did not have the unspooling problem seen in Batch 1. However, a new problem was observed which may have escaped detection in Batch 1. The new problem is the folding of the tow onto itself across the width, resulting in variable tow width. This problem is illustrated in a photograph of a ±45° tube in Figure 18. The gap is shown clearly because of the contrasting color of the mandrel. While the gaps in the first layer wound onto the heated mandrel could be "fixed" to some degree by spreading the warmed tow manually, in the subsequent layers it was not possible to see the gaps by eye. The folds were visible in the towpreg as it came off the spool. This phenomenon was not seen in the uncoated towpreg.

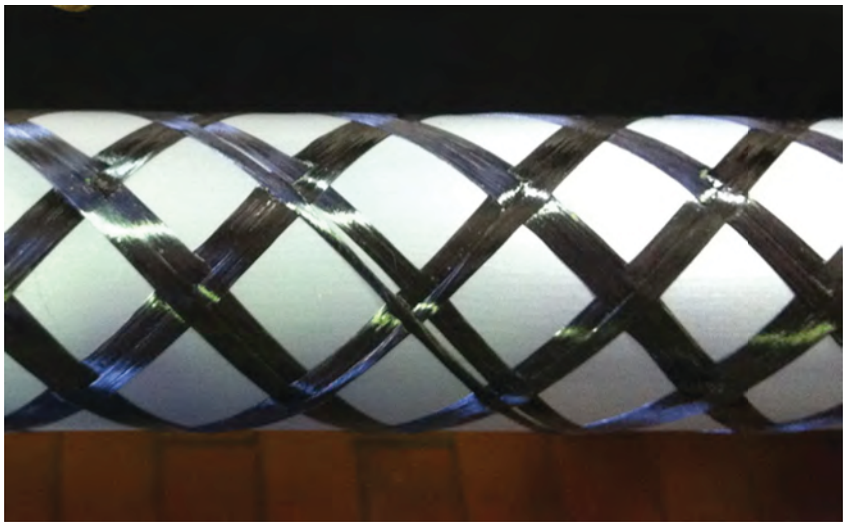

Figure 18.—Winding of a ±45° tube showing a folded-over tow and non-uniform tow width.

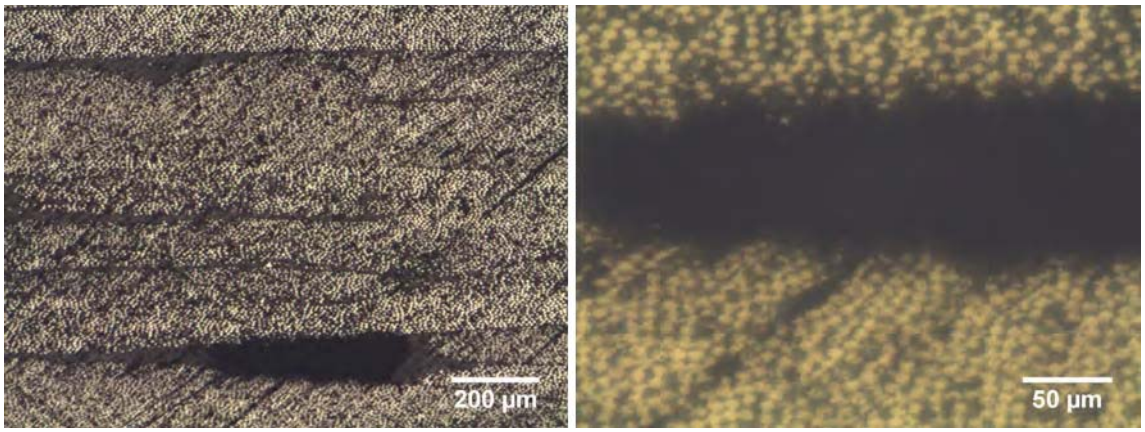

Figure 19.—Void shown in a 45° tube (left), higher magnification of the region around the same void (right).

Some voids were observed in the ±45° tubes (Figure 19), which are believed to be related to the folded tows and resulting gaps that formed between tows as they were deposited onto the mandrel. During the 90° winding, similar tow width problems were observed during winding, but large voids were not detected in the cured tubes. It is believed that the 90° layers can "nest" better among themselves, in comparison to the ±45° tubes, thus eliminating voids due to fiber compaction.

Variation in the wall thickness was observed in the tubes made with coated towpreg, as was the case with the unmodified material. The average difference between the thickest part of the wall and the thinnest part of wall was 0.23 mm in the ±45° specimens and 0.09 mm in the hoop-wound specimens. Appendix B summarizes wall thickness measurements made at the top and bottom ends of each specimen. In comparing the measurements in Appendix B with those for the tubes made with uncoated towpreg (Appendix A), it is seen that the coating process adds a few hundredths of a millimeter to the wall thickness of the tubes. The variability in wall thickness was unaffected, however.

Testing and Characterization

The materials were characterized at several steps during this work. Preliminary microscopy was used to check the suitability of the electrospinning precursor solutions but is not included. Scanning electron microscopy (SEM) was used to image the nanofiber after it was deposited on the carbon tow and after the tubes specimens were fabricated. Finally, mechanical tests were performed on the ±45 and 90 specimens that included tension and compression. This section will cover these results.

Deposited Nanofiber

Scanning electron microscopy (SEM) was used to image the as-deposited nanofiber on the surface of the carbon fiber towpreg and in a cut sample of cured composite. The expected random mesh was observed on the towpreg surface. Measurements of the nanofiber diameters ranged from 100 to 300 nm before and after composite fabrication. Figure 20 shows the deposited nanofiber mesh pressed into the resin on the surface of the carbon fiber towpreg. SEM images of the nanofiber in cured composite are included in Appendix D. The carbon fiber is not visible.

Figure 21 shows the nanofiber mesh spanning ridges on the surface of the carbon fiber towpreg (left) and a close up showing the resin wicking onto the nanofiber mesh (right).

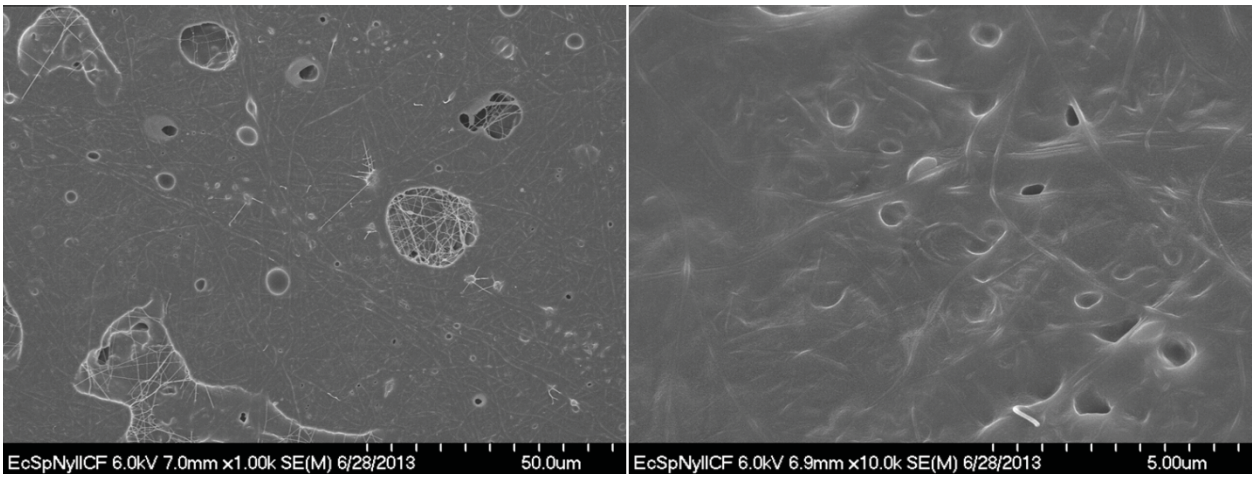

Figure 20.—SEM images showing the electrospun nanofiber pressed into the resin on the towpreg surface after deposition (left), increased magnification (right).

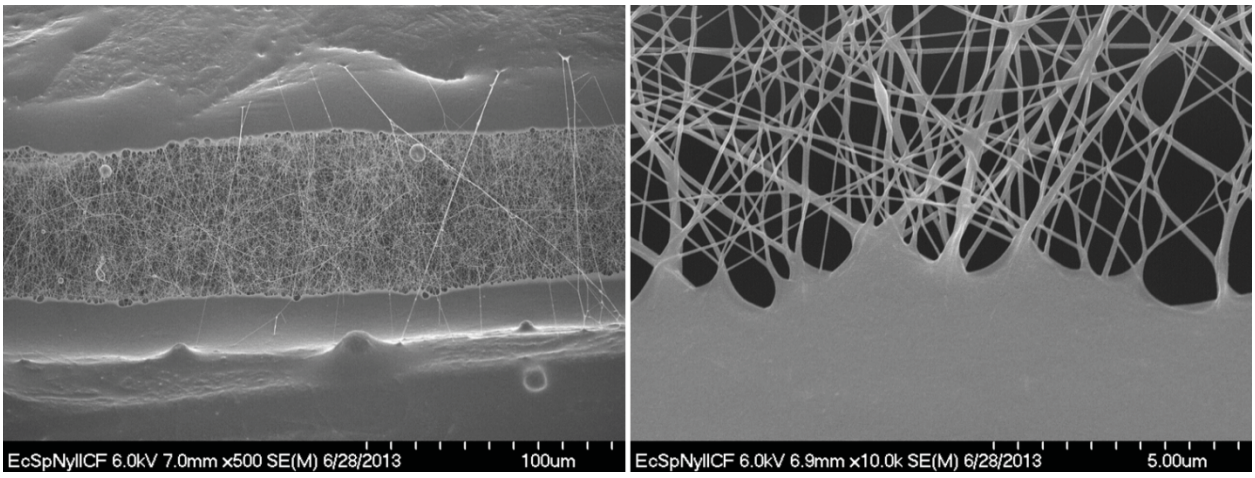

Figure 21.—SEM images showing the nanofiber mesh spanning surface ridges on the carbon fiber towpreg (left) and a close up showing the resin wicking onto the nanofiber mesh (right).

Mechanical Testing

Mechanical strength tests were performed using a screw-driven electromechanical load frame, Instron model 1125 with an MTS Sintech Upgrade Package. The machine was equipped with MTS 647 hydraulic wedge grips. For the tension and compression tests, a displacement rate of 0.05 in./min was used. The tensile tube coupons were bonded into stainless steel end caps using Loctite Hysol E-60HP 2 part epoxy. Five sets of end caps were fabricated so that all specimens of each set could be bonded and tested together. Following each test set, the center section of the tube was cut out and the end caps with the ends still bonded in were burned out at 450 °C for 6 to 8 hr and the remaining residue removed by abrasive grit blasting. A complete tensile specimen is shown in Figure 22 (top) and a section view of the assembly (bottom). The ends of the assembly are threaded to interface with calibration hardware adapters that were used to interface with the wedge grips in the machine.

The ±45° tensile specimens deformed significantly (radial contraction) following the onset of nonlinearity above 8000 lb (35.6 kN) load (Appendix C). Ultimate failure was characterized by a peak in load followed by an extended unloading (negative load/displacement curve slope) resulting from progressive delamination of the tows. The 90° tensile specimens failed at the end cap bond line at relatively low load with no nonlinear deformation as anticipated. Figure 23 shows a ±45° tensile specimen after failure, still mounted in the load frame.

The ends of the compression coupons were cut flat and parallel using a precision diamond saw. Steel end plates with a shallow channel (0.125 in. deep by 0.125 in. wide with a mean diameter of 1.985 in. or 3.175 mm deep by 3.175 mm wide with a mean diameter of 50.419 mm) were used on the ends of the coupons. The end plates were not bonded to the specimens. The coupon with loose fitting end plates was placed in the test machine between flat compression platens. Figure 24 shows the compression test end plates and a ±45 specimen.

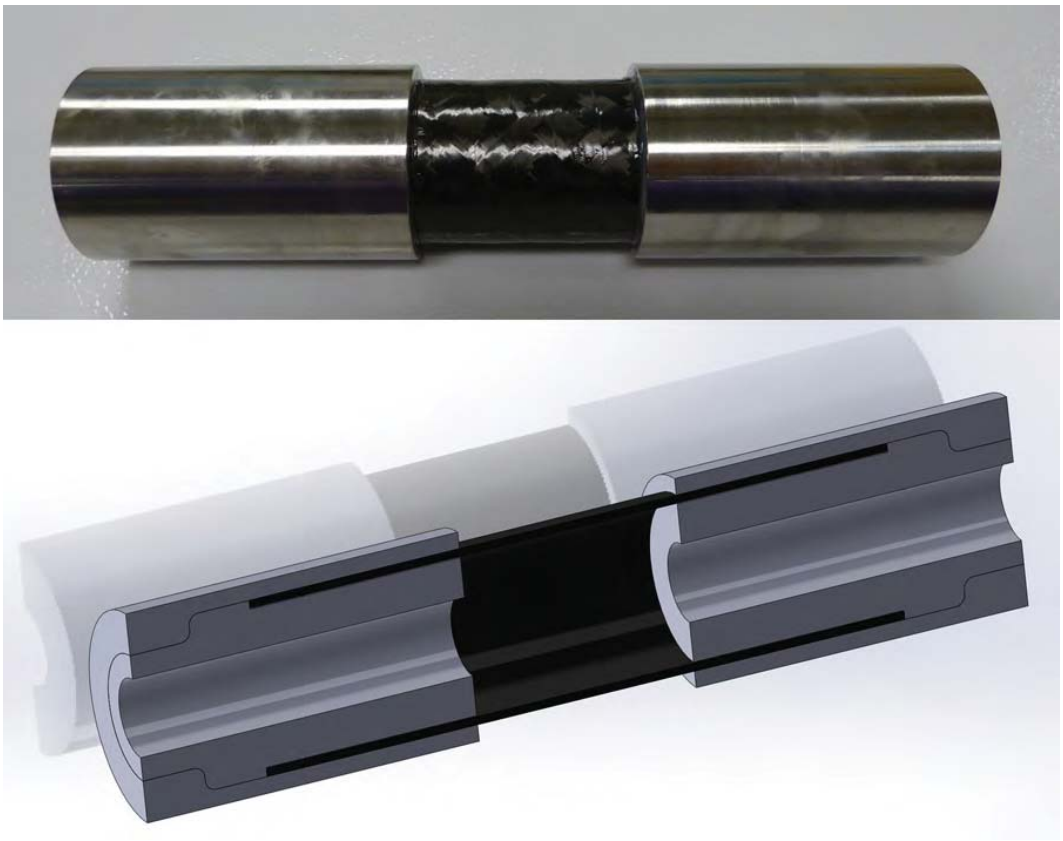

Figure 22.—Finished tensile specimen (top) and section view of assembly (bottom).

Figure 23.—Failed ±45 tension specimen still mounted in test machine.

Figure 24.—Compression test end plates and ±45 specimen.

Figure 25.—Examples of compression specimen failures, ±45 (left) and 90 (right).

The ±45° compression specimens show a significant change in stiffness (softening) at higher load that was associated with severe barreling of the tube. The final failure resulted in fractures running along the 45° directions of the fibers, often near one of the end plates. The 90° tubes showed significantly less non-linearity. The compression specimens typically failed toward the middle of the specimen and resulted in broken hoop direction fibers and a local ring of compression damage. Examples of the failure of ±45 and 90 compression test specimens are shown in Figure 25.

The load-displacement curves for the coupon tests are shown in Appendix C. The peak load for each specimen was recorded and the average and standard deviations computed. Figure 26 shows the measured tension strengths with error bars representing two times the standard deviation. The baseline values are shown in blue and the modified tube values shown in red. The numbers in the bottom of each bar indicate the number of specimens used in the computations.

Figure 27 shows the measured compression strengths with error bars representing two times the standard deviation. The baseline values are shown in blue and the modified tube values shown in red. The numbers in the bottom of each bar indicate the number of specimens used in the computations. The ±45° tension tubes with the added nanofiber toughener shows an increase in average strength of 11.6 percent over baseline with two times the standard deviation of baseline and modified set not showing an overlap. The average strengths of the remaining modified test sets show no significant difference as compared to the baselines when the standard deviation overlaps are considered. This is true not only for two times standard deviation but one standard deviation as well. This is because the main driver for ultimate failure of the ±45° tension tube is interlaminar shearing of the tow to tow interface, whereas the other specimens undergo different failure mechanisms including in-plane shear and transverse tension that are less affected by the nanofiber toughener.

The lack of change in the 90° tension specimens may imply poor bonding of the nanofiber to the matrix material or that an insignificant quantity is present to appreciably affect the transverse tensile strength of the composite. Additional testing is needed to further investigate the adhesion of the epoxy matrix to the polymer nanofiber.

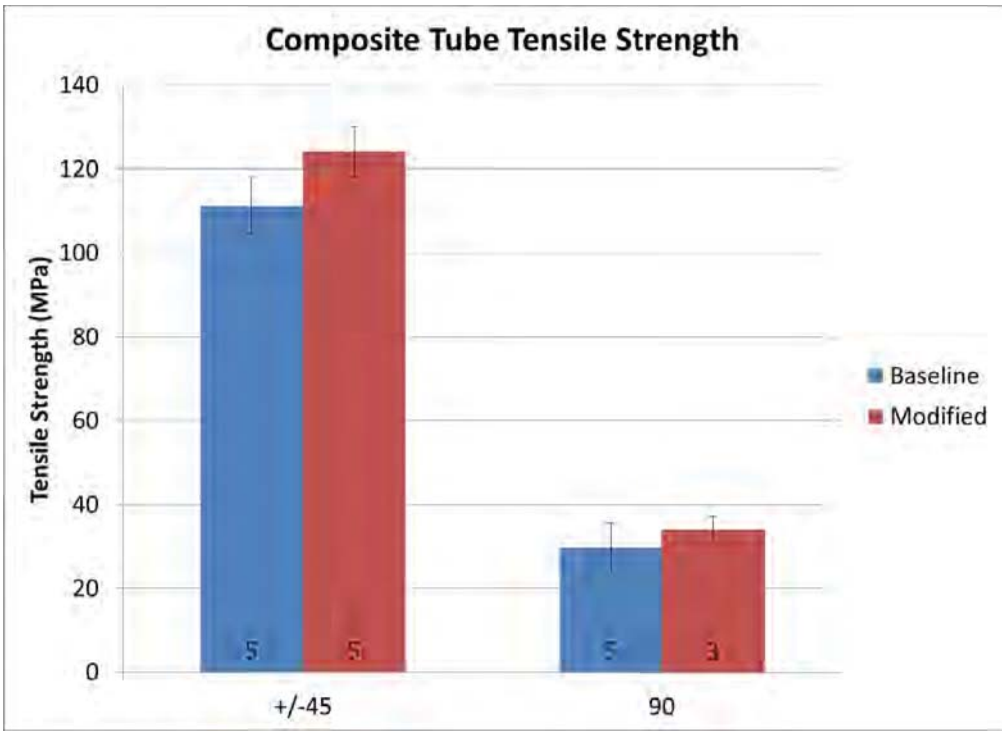

Figure 26.—Average peak stress for tension specimens, error bars represent two times standard deviation, the number of specimens appear in the bottom of each bar, baseline (blue) and modified (red).

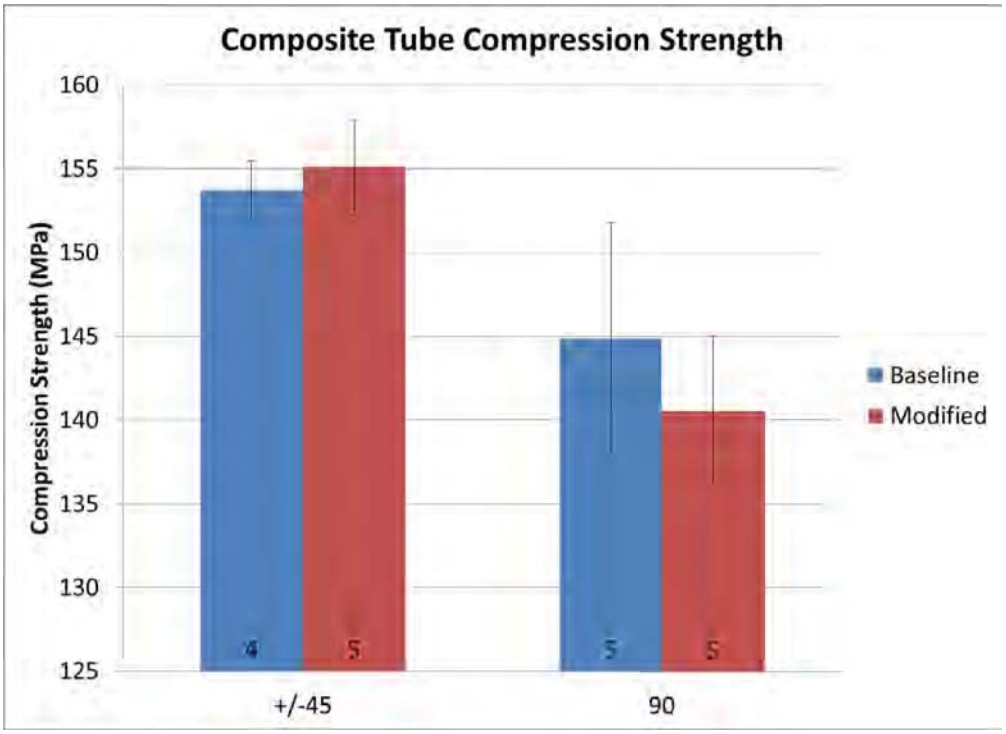

Figure 27.—Average peak stress for compression specimens, error bars represent two times standard deviation, the number of specimens appear in the bottom of each bar, baseline (blue) and modified (red).

Summary

The use of direct electrospun deposition of thermoplastic nanofibers on continuous carbon material for toughening of composites was demonstrated. The process was first demonstrated at small scale and then using a larger continuous lab scale process that resulted in the production of roughly 12,000 ft (3658 m) of nanofiber coated towpreg. The coated material was used to fabricate tension and compression coupons with ±45° and hoop wound 90° architectures. Aside from the ±45 tension coupons, no change was observed in the strength measurements. The ±45 tension coupons however, showed an increase of 11.6 percent in tensile strength compared to the baseline material. No overlap in two times the standard deviation of each test set was observed. More work is needed to improve the deposition process. Investigation of the compatibility and suitability of different thermoplastic nanofiber materials could result in more significant improvements in interface toughness and therefore composite strength.

Appendix A.—Wall Thickness Measurements of Baseline Tubes

Specimen identification notation:

45 (or 90)	Winding angle
UM	Unmodified prepreg (no nanofibers)
T	Tension test specimen
C	Compression test specimen

TABLE 5.—UNMODIFIED $[\pm 45]_4$ TUBES

Specimen ID		Minimum (mm)	Maximum (mm)	Max-Min (mm)
45-UM-T1	Top	2.24	2.50	0.26
	Bottom	2.22	2.40	0.18
45-UM-T2	Top	2.16	2.54	0.38
	Bottom	2.26	2.52	0.26
45-UM-T3	Top	2.26	2.48	0.22
	Bottom	2.16	2.50	0.34
45-UM-T4	Top	2.14	2.50	0.36
	Bottom	2.14	2.50	0.36
45-UM-T5	Top	2.20	2.46	0.26
	Bottom	2.02	2.52	0.50
45-UM-C1	Top	2.28	2.48	0.20
	Bottom	2.28	2.44	0.16
45-UM-C2	Top	2.30	2.48	0.18
	Bottom	2.26	2.46	0.20
45-UM-C3	Top	2.26	2.42	0.16
	Bottom	2.26	2.46	0.20
45-UM-C4	Top	2.28	2.48	0.20
	Bottom	2.30	2.50	0.20
45-UM-C5	Top	2.12	2.48	0.36
	Bottom	2.18	2.50	0.32
45-UM-C6	Top	2.26	2.44	0.18
	Bottom	2.32	2.46	0.14
45-UM-C7	Top	2.26	2.44	0.18
	Bottom	2.24	2.42	0.18
45-UM-C8	Top	2.20	2.40	0.20
	Bottom	2.22	2.42	0.20
45-UM-C9	Top	2.26	2.48	0.22
	Bottom	2.24	2.48	0.24
45-UM-C10	Top	2.14	2.52	0.38
	Bottom	2.16	2.50	0.34
	Avg.	2.22	2.47	0.25

TABLE 6.—UNMODIFIED $[90]_9$ TUBES

Specimen ID		Minimum (mm)	Maximum (mm)	Max-Min (mm)
90-UM-T1	Top	2.36	2.42	0.06
	Bottom	2.32	2.42	0.10
90-UM-T2	Top	2.28	2.36	0.08
	Bottom	2.22	2.34	0.12
90-UM-T3	Top	2.22	2.34	0.12
	Bottom	2.22	2.32	0.10
90-UM-T4	Top	2.16	2.28	0.12
	Bottom	2.16	2.28	0.12
90-UM-T5	Top	2.18	2.26	0.08
	Bottom	2.16	2.26	0.10
90-UM-C1	Top	2.20	2.30	0.10
	Bottom	2.20	2.28	0.08
90-UM-C2	Top	2.20	2.28	0.08
	Bottom	2.22	2.26	0.04
90-UM-C3	Top	2.26	2.34	0.08
	Bottom	2.26	2.32	0.06
90-UM-C4	Top	2.18	2.26	0.08
	Bottom	2.18	2.28	0.10
90-UM-C5	Top	2.22	2.30	0.08
	Bottom	2.22	2.34	0.12
90-UM-C6	Top	2.28	2.38	0.10
	Bottom	2.24	2.36	0.12
90-UM-C7	Top	2.18	2.26	0.08
	Bottom	2.16	2.24	0.08
90-UM-C8	Top	2.18	2.24	0.06
	Bottom	2.18	2.24	0.06
90-UM-C9	Top	2.18	2.24	0.06
	Bottom	2.18	2.24	0.06
90-UM-C10	Top	2.20	2.28	0.08
	Bottom	2.20	2.26	0.06
	Avg.	2.21	2.30	0.09

Appendix B.—Wall Thickness Measurements of Modified Tubes

Specimen identification notation:

45 (or 90) Winding angle
M Modified towpreg (nanofiber coating)
T Tension test specimen
C Compression test specimen

TABLE 7.—MODIFIED $[\pm 45]_4$ TUBES

Specimen ID		Minimum (mm)	Maximum (mm)	Max-Min (mm)
45-M-T1	Top	2.39	2.62	0.23
	Bottom	2.26	2.44	0.18
45-M-T2	Top	2.26	2.49	0.23
	Bottom	2.26	2.51	0.25
45-M-T3	Top	2.26	2.51	0.25
	Bottom	2.24	2.41	0.17
45-M-T4	Top	2.36	2.51	0.15
	Bottom	2.24	2.57	0.33
45-M-T5	Top	2.26	2.57	0.31
	Bottom	2.29	2.51	0.22
45-M-C1	Top	2.29	2.41	0.12
	Bottom	2.26	2.46	0.2
45-M-C2	Top	2.24	2.54	0.3
	Bottom	2.24	2.51	0.27
45-M-C3	Top	2.26	2.46	0.2
	Bottom	2.24	2.51	0.27
45-M-C4	Top	2.31	2.49	0.18
	Bottom	2.29	2.49	0.2
45-M-C5	Top	2.26	2.59	0.33
	Bottom	2.31	2.57	0.26
45-M-C6	Top	2.29	2.46	0.17
	Bottom	2.24	2.49	0.25
45-M-C7	Top	2.24	2.46	0.22
	Bottom	2.26	2.46	0.2
45-M-C8	Top	2.21	2.46	0.25
	Bottom	2.24	2.49	0.25
45-M-C9	Top	2.24	2.51	0.27
	Bottom	2.21	2.49	0.28
45-M-C10	Top	2.24	2.49	0.25
	Bottom	2.24	2.46	0.22
	AVG	2.26	2.50	0.23

TABLE 8.—$[90]_9$ TUBES

Specimen ID		Minimum (mm)	Maximum (mm)	Max-Min (mm)
90-M-T1	Top	2.31	2.46	0.15
	Bottom	2.29	2.41	0.12
90-M-T2	Top	2.26	2.41	0.15
	Bottom	2.26	2.41	0.15
90-M-T3	Top	2.29	2.41	0.12
	Bottom	2.29	2.41	0.12
90-M-T4	Top	2.31	2.41	0.1
	Bottom	2.31	2.41	0.1
90-M-T5	Top	2.31	2.41	0.1
	Bottom	2.29	2.41	0.12
90-M-C1	Top	2.24	2.31	0.07
	Bottom	2.26	2.36	0.1
90-M-C2	Top	2.34	2.36	0.02
	Bottom	2.26	2.34	0.08
90-M-C3	Top	2.24	2.34	0.1
	Bottom	2.24	2.36	0.12
90-M-C4	Top	2.29	2.41	0.12
	Bottom	2.26	2.41	0.15
90-M-C5	Top	2.29	2.36	0.07
	Bottom	2.26	2.31	0.05
90-M-C6	Top	2.34	2.39	0.05
	Bottom	2.26	2.31	0.05
90-M-C7	Top	2.24	2.36	0.12
	Bottom	2.31	2.36	0.05
90-M-C8	Top	2.34	2.39	0.05
	Bottom	2.34	2.39	0.05
90-M-C9	Top	2.36	2.41	0.05
	Bottom	2.34	2.39	0.05
90-M-C10	Top	2.31	2.36	0.05
	Bottom	2.39	2.44	0.05
	AVG	2.29	2.38	0.09

Appendix C.—Load Displacement Curves of Test Coupons

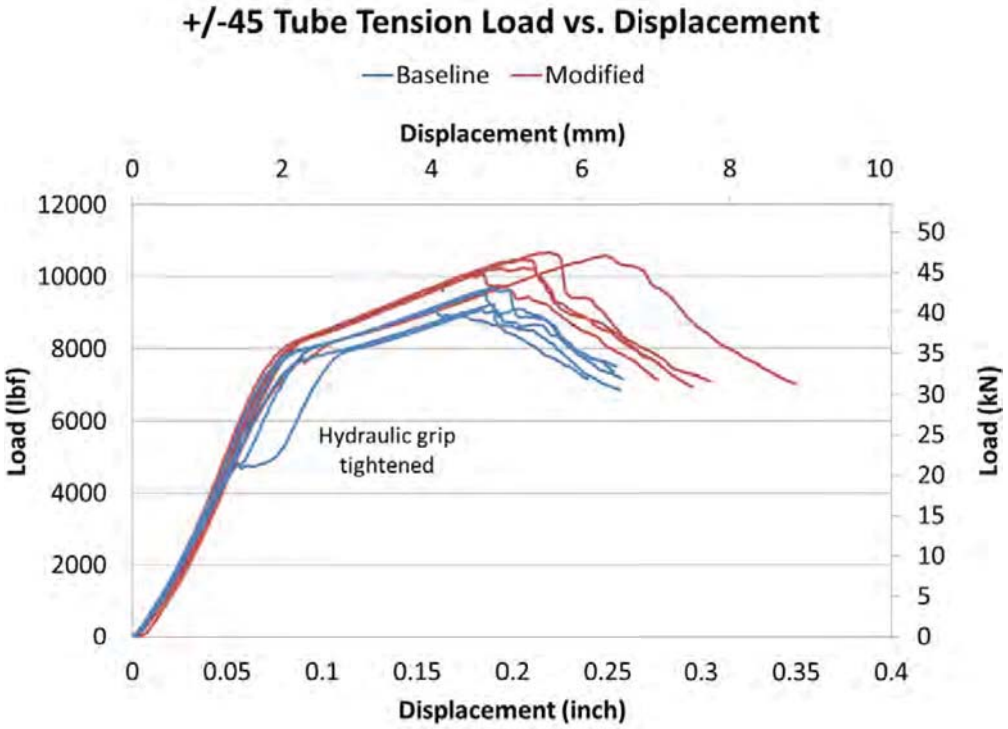

Figure 28.—Load vs. displacement curves for all tubes with the ±45° wind angle loaded in tension.

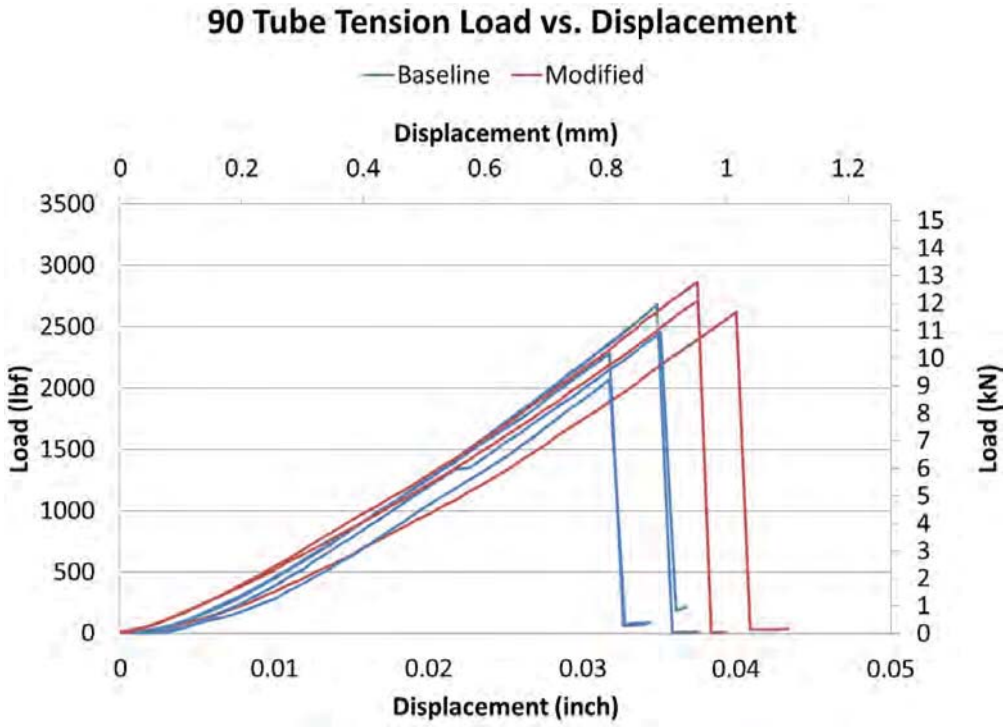

Figure 29.—Load vs. displacement curves for all tubes with the 90° wind angle loaded in tension.

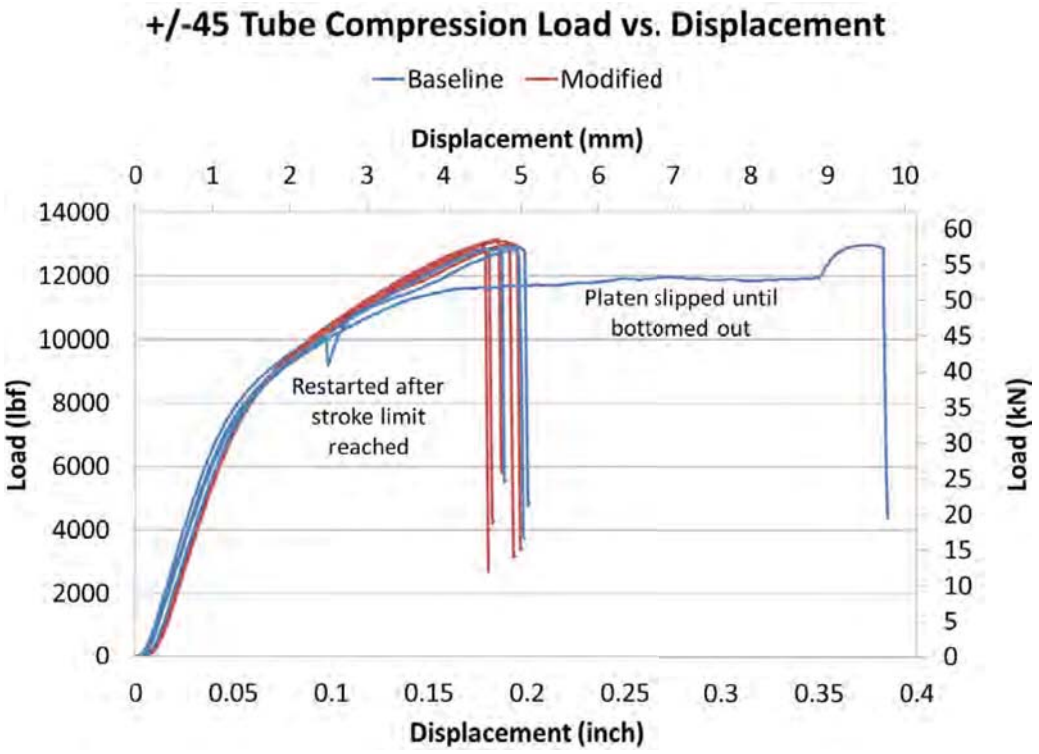

Figure 30.—Load vs. displacement curves for all tubes with the ±45° wind angle loaded in compression.

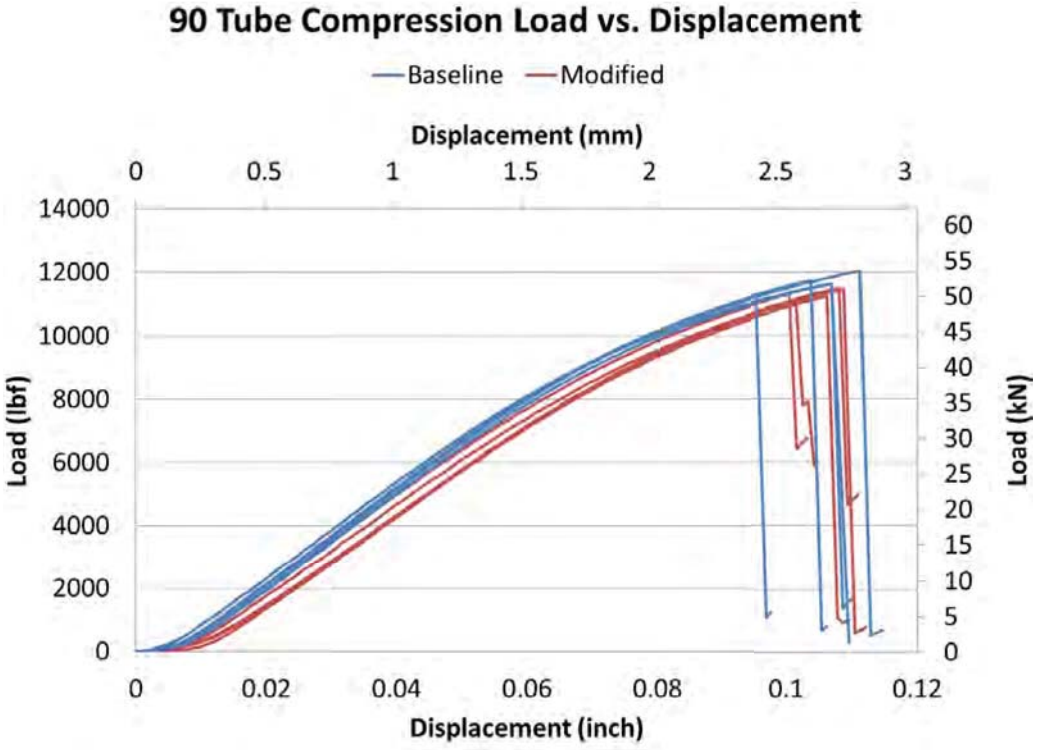

Figure 31.—Load vs. displacement curves for all tubes with the 90° wind angle loaded in compression.

Appendix D.—Scanning Electron Microscopy of Electrospun Nanofibers in Cured Composite

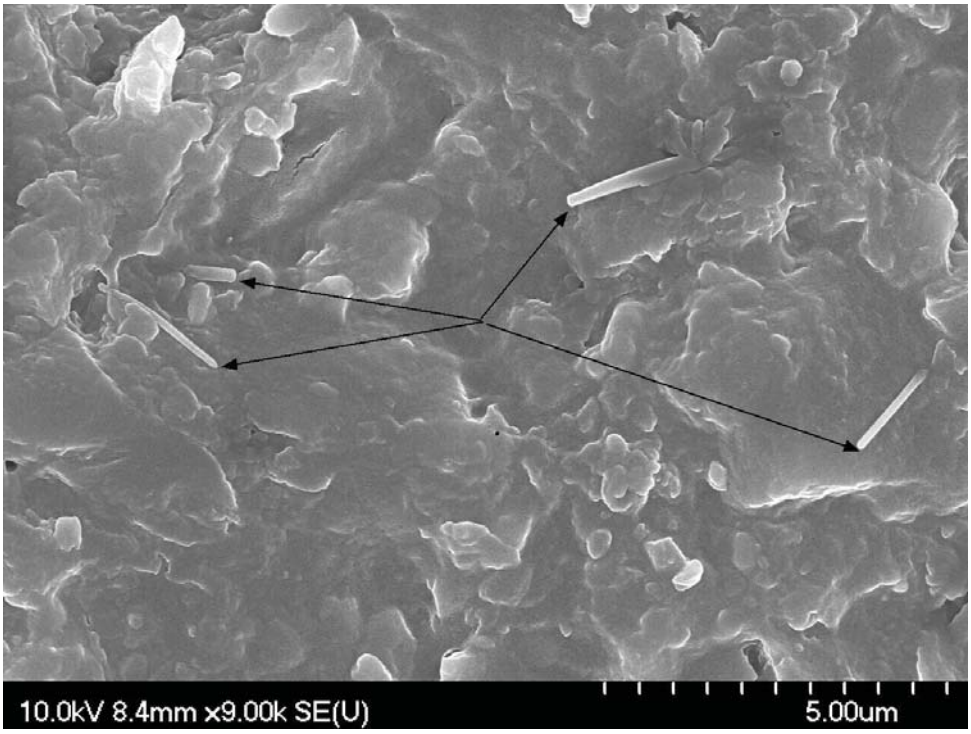

Figure 32.—Scanning electron microscopy image of electrospun nanofibers protruding from cut surface of cured composite.

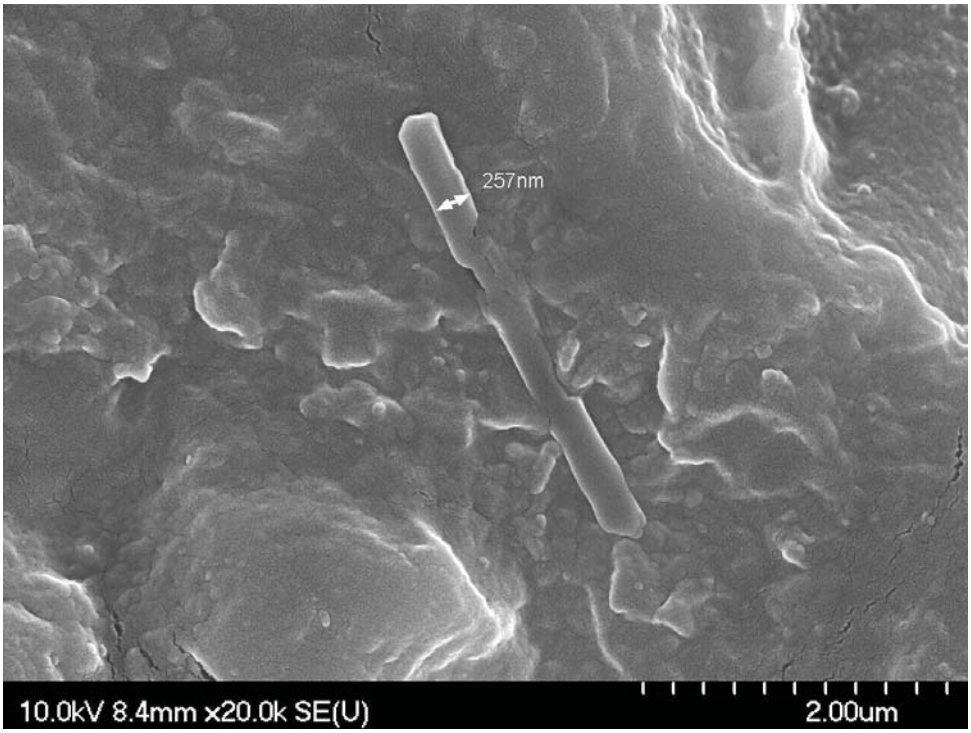

Figure 33.—Scanning electron microscopy image of electrospun nanofiber protruding from cut surface of cured composite, diameter measured at 257 nm.

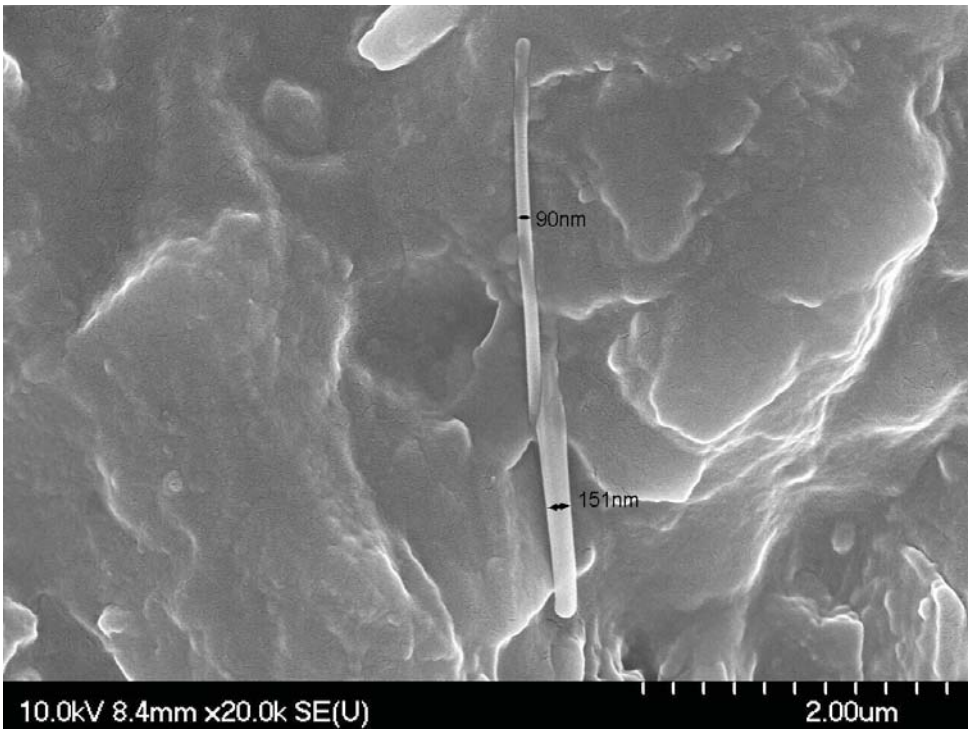

Figure 34.—Scanning electron microscopy image of electrospun nanofibers protruding from cut surface of cured composite, diameters measured at 90 and 151 nm.

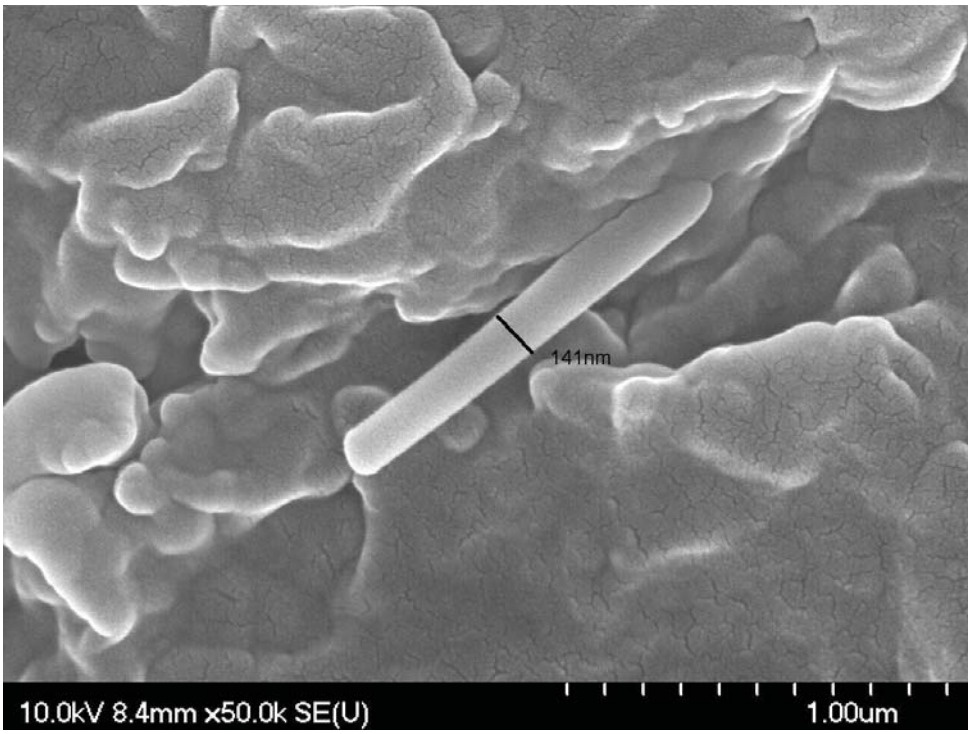

Figure 35.—Scanning electron microscopy image of electrospun nanofiber protruding from cut surface of cured composite, diameter measured at 141 nm.

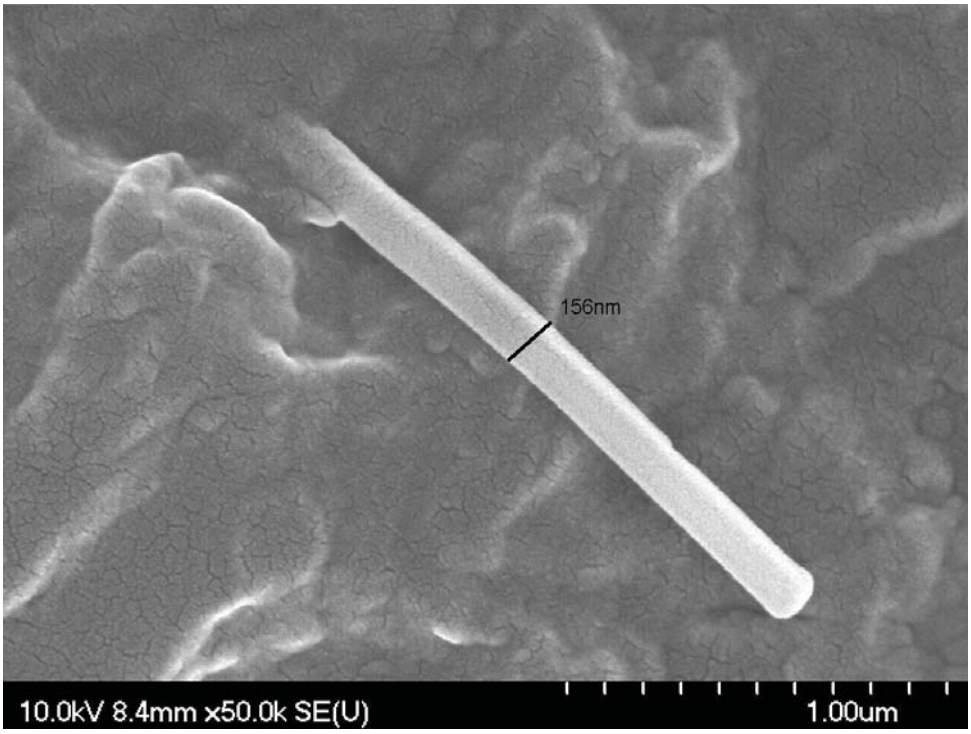

Figure 36.—Scanning electron microscopy image of electrospun nanofiber protruding from cut surface of cured composite, diameter measured at 156 nm.

References

Andersons, J., and M. König. Dependence of fracture toughness of composite laminates on interface ply orientations and delamination growth direction. Composites Science and Technology, 64 (2004) 2139–2152.

Bhattacharjee, P.K., and G.C. Rutledge. Electrospinning and polymer nanofibers: Process Fundamentals. Comprehensive Biomaterials, Volume 1: Metallic, Ceramic and Polymeric Biomaterials, (2011) 497–512.

Behler, K., Havel, M., and Gogotsi, Y. New solvent for polyamides and its application to the electrospinning of polyamides 11 and 12. Polymer, 48 (2007) 6617–6621.

Homaeigohar, S.S., K. Buhr, and K. Ebert. Polyethersulfone electrospun nanofibrous composite membrane for liquid filtration. Journal of Membrane Science, Volume 365, Issue 1-2, December 1, 2010, 68–77 http://dx.doi.org/10.1016/j.memsci.2010.08.041.

Tang, Z., C. Qiu, J. R. McCutcheon, K. Yoon, H. Ma, D. Fang, E. Lee, C. Kopp, B.S. Hsiao, and B. Chu. Design and fabrication of electrospun polyethersulfone nanofibrous scaffold for high-flux nanofiltration membranes. Journal of Polymer Science: Part B: Polymer Physics, 47 (2009) 2288–2300.